SCATTERING FROM SUPERQUADRIC SURFACES

L.A. Takacs
R.J. Marhefka

The Ohio State University
ElectroScience Laboratory

Department of Electrical Engineering
Columbus, Ohio 43212

Technical Report No. 718422-2
Contract No. N60530-85-C-0249
June 1988

Department of the Navy
Naval Weapons Center
China Lake, California 93555-6001

and

Harry Diamond Labs
2800 Powder Mill Road
Adelphi, Maryland 20783-119[illegible]

NOTICES

When Government drawings, specifications, or other data are used for any purpose other than in connection with a definitely related Government procurement operation, the United States Government thereby incurs no responsibility nor any obligation whatsoever, and the fact that the Government may have formulated, furnished, or in any way supplied the said drawings, specifications, or other data, is not to be regarded by implication or otherwise as in any manner licensing the holder or any other person or corporation, or conveying any rights or permission to manufacture, use, or sell any patented invention that may in any way be related thereto.

50272-101

REPORT DOCUMENTATION PAGE	1. REPORT NO.	2.	3. Recipient's Accession No

4. Title and Subtitle

SCATTERING FROM SUPERQUADRIC SURFACES

5. Report Date
June 1988

6.

7. Author(s)
L.A. Takacs and R.J. Marhefka

8. Performing Organization Rept No
718422-2

9. Performing Organization Name and Address

The Ohio State University ElectroScience Laboratory
1320 Kinnear Road
Columbus, Ohio 43212

10. Project/Task/Work Unit No

11. Contract(C) or Grant(G) No
(C) N60530-85-C-0249
(G)

12. Sponsoring Organization Name and Address

Department of the Navy
Naval Weapons Center
China Lake, California 93555-6001

Harry Diamond Labs
2800 Powder Mill Road
Adelphi, Maryland 20783-1193

13. Type of Report & Period Covered
Technical

14.

15. Supplementary Notes

16. Abstract (Limit: 200 words)

Electromagnetic reflection from superquadric surfaces in 2-D is examined. A finite number of zero-curvature points on the surface are identified, and Geometrical Optics is shown to fail at these points. A correction for the failure, based on Physical Optics, is derived via an asymptotic approximation of the PO radiation integral. Solutions are obtained for two cases: reflection from the zero-curvature point for all values of the superquadric parameter ν, and reflection both near and far from the zero-curvature point when $\nu = 3$. The form of the general multiplicative transition (correction) function is postulated heuristically, based on the integral form of a generalized incomplete Airy function. The resulting Uniform Geometrical Optics (UGO) result compares very favorably with Physical Optics and the Method of Moments.

17. Document Analysis a. Descriptors

b. Identifiers/Open-Ended Terms

c. COSATI Field/Group

18. Availability Statement
Approved for public release; distribution is unlimited.

19. Security Class (This Report)
Unclassified

21. No. of Pages
98

20. Security Class (This Page)
Unclassified

22. Price

(See ANSI-Z39.18) See Instructions on Reverse OPTIONAL FORM 272 (4-77)
(Formerly NTIS-35)
Department of Commerce

Contents

List of Figures

List of Tables

Chapter 1

INTRODUCTION

The electromagnetic scattering from a subclass of superquadric surfaces, specifically two-dimensional, perfectly conducting superelliptic cylinders is treated. Scattering may be defined as the modification of the electromagnetic radiation fields due to the presence of complex geometries.

Computer modeling is an active area of high-frequency electromagnetic research. It concerns itself with the construction of efficient computer programs to calculate values for the various antenna and radar cross-section parameters of complex antennas and scatterers. Some of these computer codes [14],[15] are capable of modeling quite complicated antennas and scatterers such as reflectors, ships, aircraft, spacecraft and many other actual structures.

The purpose of this report is to extend the scope of computer modeling codes to include superquadric shapes in order to represent complex geometries by a new class of analytic functions. Superquadrics show great promise of providing researchers and engineers with a powerful family of parametric shapes for geometrical modeling. One of the main problem areas today in

modeling is the lack of a unified mathematical formalism and specification language for geometrical objects. By providing modelers with the facility to generate a wide variety of shapes from a small number of intuitive parameters, superquadrics may prove to be a step in the right direction toward the needed mathematical basis. Since superquadrics allow complex surfaces to be generated and modified easily and interactively, there is also hope that they would integrate naturally with an evolving specification language for geometrical objects.

This report, then, represents a small step in examining the potential of these surfaces for this purpose.

Chapter 2

THEORETICAL BACKGROUND

2.1 Introduction

The solutions of electromagnetic problems consist of solutions to Maxwell's equations and the equation of continuity, together with appropriate boundary conditions. There are three high-frequency techniques of particular interest here, Physical Optics (PO), Geometrical Optics (GO) and the Uniform (Geometrical) Theory of Diffraction (UTD).

2.2 Geometrical Optics (GO)

Geometrical Optics is an approximate technique tha' can be used to represent radiated, reflected, and refracted fields. GO can be derived via an asymptotic series (Luneburg-Kline) solution of the Maxwell's equations; the leading term of the series is the GO field.

The GO field is discontinuous across a shadow boundary. Its amplitude is governed by the conservation of energy in a ray tube as it travels along

the ray path. The phase is proportional to the length of the ray path, and ray tubes are defined by surfaces normal to the ray path through which the flow of power is a constant. GO fails when the energy of a ray tube must pass through a point or line. Such points and lines are called caustics, and they signal the attempt by GO to represent the flow of a finite amount of power through a vanishing area. In two dimensions, the GO reflected field is

$$E_z^r(\vec{r}) = -E_z^i(Q_r) \cdot \sqrt{\frac{\rho^r}{(\rho^r + s^r)}} e^{-jks^r} \tag{2.1}$$

$$H_z^r(\vec{r}) = +H_z^i(Q_r) \cdot \sqrt{\frac{\rho^r}{(\rho^r + s^r)}} e^{-jks^r} \tag{2.2}$$

where

$$\begin{aligned}
Q_r &= \text{reflection point} \\
E_z^i(Q_r) &= \text{incident } E_z \text{ field at } Q_r \\
H_z^i(Q_r) &= \text{incident } H_z \text{ field at } Q_r \\
s^i &= \text{distance from } Q_r \text{ to source} \\
s^r &= \text{distance from } Q_r \text{ to receiver} \\
\rho^r &= \text{caustic distance for the reflected ray} \\
\frac{1}{\rho^r} &= \frac{1}{\rho^i} + \frac{2}{R_c(Q_r)\cos\theta^i} \\
\frac{1}{\rho^i} &= \text{caustic distance for the incident ray} \\
\theta^i &= \text{angle of incidence} = \cos^{-1}(-\hat{s}^i \cdot \hat{n}) \\
R_c(Q_r) &= \text{principal radius of surface curvature at } Q_r. \\
\hat{n} &= \text{normal to the surface at } Q_r \\
\hat{t} &= \text{tangent to the surface at } Q_r
\end{aligned}$$

$\hat{s}^i$ = direction of the incident ray

$\hat{s}^r$ = direction of the reflected ray

$\hat{r}'$ = direction of the source

$\hat{r}$ = direction of the receiver

as can be seen in Figure 2.1. The direction of the reflected ray is defined

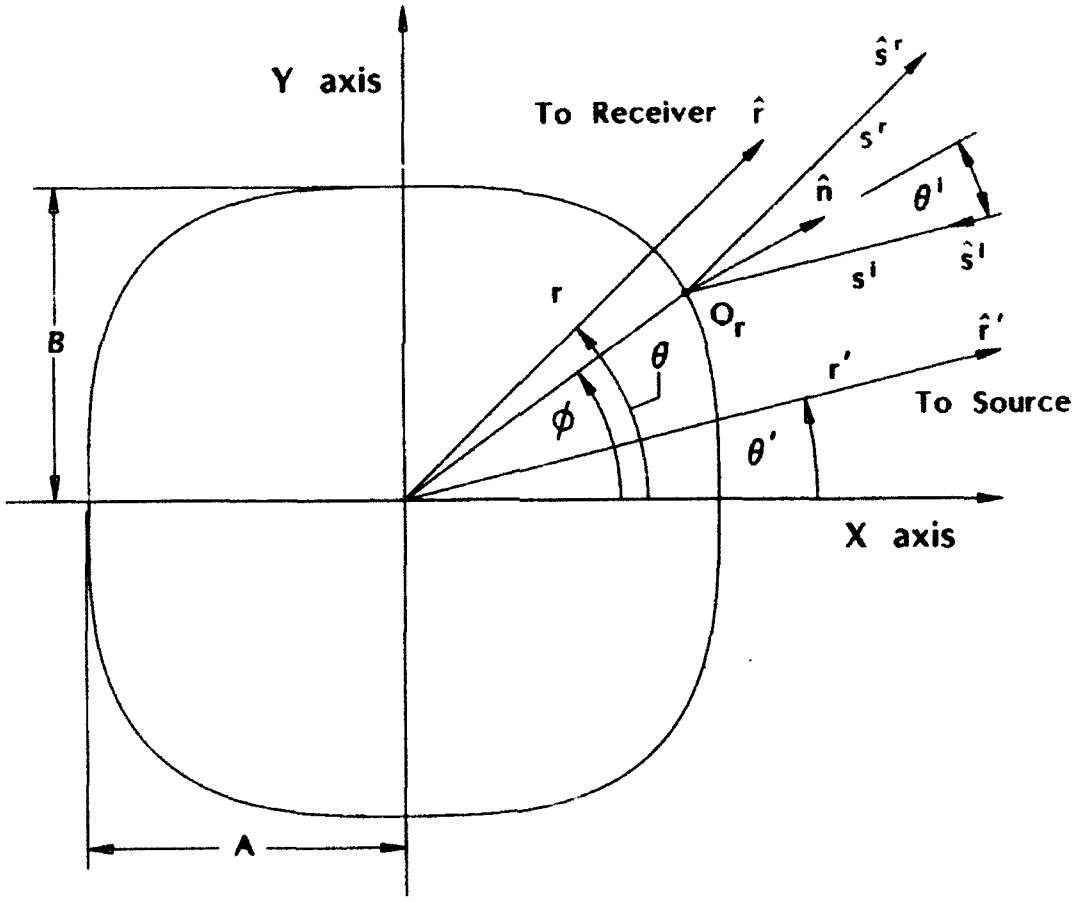

Figure 2.1: Geometry for the GO Reflected Field

by the law of reflection and is

$$\hat{n} \cdot \hat{s}^r = -\hat{n} \cdot \hat{s}^i. \tag{2.3}$$

The point of reflection, Q_r, is a point on the surface such that the law of reflection is satisfied. For far field scattering from Q_r, $\hat{n} \cdot \hat{r} = \hat{n} \cdot \hat{r}'$.

2.3 The Physical Optics Procedure (PO)

The currents induced on a general scatterer are unknown. If the true currents were known, then exact field values could be calculated using the radiation integrals [9]. Physical Optics is a procedure where unknown currents are approximated by equivalent currents based on the incident G.O. fields. The equivalence theorem allows replacement of the original scattering geometry and the actual surface currents by equivalent surface currents flowing in free space. These approximate G.O. currents are then used to calculate the scattered fields. The currents induced on the surface of a perfect electric conductor are assumed to be

$$\vec{J}_s = \begin{cases} 2\,\hat{n} \times \vec{H}^i, & \text{in the Lit region} \\ 0, & \text{in the Shadow region} \end{cases} \tag{2.4}$$

where $\hat{n}$ is the unit normal to the surface.

Physical Optics is useful because the form of the assumed currents is simple and the resulting integrals lend themselves to either numerical or asymptotic (high-frequency) analysis. It is not possible to rigorously state the conditions of validity of PO, but several guidelines may be employed when determining its validity in a given problem. In general, whenever the assumed currents are not a good approximation to the actual currents then

PO will be invalid somewhere. For example, in a bistatic scattering configuration where currents in a shadow region contribute significantly to the total field, the physical optics approximation is no longer accurate. Another source of error in the PO formulation is the assumed termination of G.O. currents on the scatterer surface. Since the actual equivalent currents do not end abruptly, evaluation of the PO integral yields contributions from the endpoints of integration which are nonphysical. When these spurious current termination contributions can be identified and removed, the PO result becomes more accurate. Care must be exercised however when determining whether a term is a false current termination or the result of a bona-fide discontinuity with physical causes.

When PO is a good approximation, and if the stationary phase condition is applicable, then a recovery of the GO result is possible from PO. Because PO is a spatial integration of surface fields, it produces bounded results in situations where the conditions required for a valid GO result do not hold. This ability of PO to treat scattering not possible with GO suggests that it represents a viable and useful format for many problems. This is the main reason that PO was chosen to characterize the scattering from superquadric surfaces.

2.4 Uniform Theory of Diffraction (UTD)

The Uniform Theory of Diffraction [10] is a uniform version of the Geometrical Theory of Diffraction. The GTD is an extension of Geometrical Optics that postulates the existence of "diffracted rays". Recall that the GO field is

discontinuous. Since actual fields must be continuous, then diffracted fields are generated that eliminate this discontinuity. These diffracted fields are added to the GO fields, i.e., $U_{gtd} = U_{go} + U_{dif.}$. The postulates of GTD are very similar to those of GO.

1) The ray paths may be found as a generalization of Fermat's principle– diffraction points occur at places such that the total ray path is an extremum.

2) Diffraction like reflection and transmission is a local phenomenon at high frequencies.

3) For a diffracted ray, power is conserved in a tube of rays and the phase of the diffracted field is proportional to the length of the traversed ray.

Generally, a UTD solution is:

- accurate
- valid at reflection and shadow boundaries and in the shadow region
- valid for an incident ray optical field with arbitrary wavefront curvature
- computationally efficient.

Chapter 3

SUPERQUADRIC SURFACES AND THEIR PROPERTIES

Superquadric surfaces are generalizations of the quadric surfaces. The definition of a quadric surface is the locus of all points (x, y, z) that satisfy the equation

$$Ax^2 + By^2 + Cz^2 + Dxy + Exz + Fyz + Gx + Hy + Jz + K = 0 \quad (3.1)$$

for arbitrary constants $A, B, C, D, E, F, G, H, J$ and K. In two dimensions, Equation 3.1 is

$$Ax^2 + By^2 + Dxy + Gx + Hy + K = 0. \quad (3.2)$$

Examples of quadric surfaces include the ellipsoid, the hyperboloid of one sheet, the hyperboloid of two sheets, the elliptic paraboloid, the hyperbolic paraboloid, the elliptic cone, and the quadric cylinder. Superquadrics do not satisfy Equations 3.1 and 3.2 except for certain special cases. For our

purpose, we restrict our attention to closed superelliptic and superellipsoidal surfaces.

The transition from quadrics to superquadrics is accomplished by allowing the exponential powers of x, y and z in Equation 3.1 to take on arbitrary values. The difficulty of raising negative numbers to fractional powers is resolved through the careful application of absolute value signs and sign functions. The proper combination of absolute value signs and sign functions ensures that a closed quadric surface generalizes to a closed superquadric.

To illustrate, consider the equation of a quadric ellipsoid in rectangular coordinates that meets the x, y and z axes at $\pm a$, $\pm b$ and $\pm c$.

$$\left(\frac{x}{a}\right)^2 + \left(\frac{y}{b}\right)^2 + \left(\frac{z}{c}\right)^2 = 1. \tag{3.3}$$

It is useful to write the surface equations in parametric form so that u and v are the principal directions of the surface. The position vector is then

$$\vec{r} = \hat{x}a \cdot \sin u \cos v + \hat{y}b \cdot \sin u \sin v + \hat{z}c \cdot \cos u \tag{3.4}$$

where

$$0 \leq u \leq \pi \quad \text{and} \quad 0 \leq v < 2\pi. \tag{3.5}$$

A normal to the surface is given by

$$\vec{n} = \frac{\hat{x}}{a} \cdot \sin u \cos v + \frac{\hat{y}}{b} \cdot \sin u \sin v + \frac{\hat{z}}{c} \cdot \cos u. \tag{3.6}$$

Generalizing the quadratic exponent in Equation 3.3 and taking note of the proper absolute values, we obtain the equation for a superellipsoid in

rectangular coordinates,

$$\left[\left|\frac{x}{a}\right|^{\nu_1} + \left|\frac{y}{b}\right|^{\nu_1}\right]^{\nu_2/\nu_1} + \left|\frac{z}{c}\right|^{\nu_2} = 1 \tag{3.7}$$

for which the components in parametric form are

$$\begin{aligned} x &= a \cdot |\sin u|^{(2/\nu_2)} \cdot |\cos v|^{(2/\nu_1)} \cdot \text{sign}\,[\sin u \cos v] \\ y &= b \cdot |\sin u|^{(2/\nu_2)} \cdot |\sin v|^{(2/\nu_1)} \cdot \text{sign}\,[\sin u \sin v] \\ z &= c \cdot |\cos u|^{(2/\nu_2)} \cdot \text{sign}\,[\cos u]\,. \end{aligned} \tag{3.8}$$

Note that in three dimensions the superellipsoid can have two different "squareness" parameters ν_1 and ν_2 applied to the principal directions u and v. Note also that the sign[] function restores the proper sign removed by the absolute value operators. For brevity, the use of absolute values is dropped in presenting the normal to the surface of the superellipsoid,

$$\vec{n} = \frac{\hat{x}}{a}(\sin u)^{2-2/\nu_2}(\cos v)^{2-2/\nu_1} + \frac{\hat{y}}{b}(\sin u)^{2-2/\nu_2}(\sin v)^{2-2/\nu_1} + \frac{\hat{z}}{c}(\cos u)^{2-2/\nu_2}. \tag{3.9}$$

Equations 3.8 and 3.9 along with similar expressions for superhyperboloids are presented in [2].

A second parametric form for the surface vector $\vec{r}(u,v)$ which satisfies a quasi-superelliptic equation

$$\left|\frac{x}{a}\right|^{\nu_1} + \left|\frac{y}{b}\right|^{\nu_1} + \left|\frac{z}{c}\right|^{\nu_2} = 1 \tag{3.10}$$

similar to Equation 3.7 is given by

$$\vec{r}(\varphi,\psi) = \hat{x}\,\frac{a \cdot \cos\psi\,(\sin\varphi)^{(\nu_2/\nu_1)}}{[((\cos\psi)^{\nu_1} + (\sin\psi)^{\nu_1})\,((\cos\varphi)^{\nu_2} + (\sin\varphi)^{\nu_2})]^{1/\nu_1}} +$$

$$+ \quad \hat{y}\,\frac{b\cdot\sin\psi\,(\sin\varphi)^{(\nu_2/\nu_1)}}{\left[\left((\cos\psi)^{\nu_1}+(\sin\psi)^{\nu_1}\right)\left((\cos\varphi)^{\nu_2}+(\sin\varphi)^{\nu_2}\right)\right]^{1/\nu_1}}+$$

$$+ \quad \hat{z}\,\frac{c\cdot\cos\varphi}{\left[(\cos\varphi)^{\nu_2}+(\sin\varphi)^{\nu_2}\right]^{1/\nu_2}} \tag{3.11}$$

where φ and ψ are used in place of u and v to indicate the alternate parameterization. This equation does not generate the same class of surfaces as Equation 3.7, but it is presented here as yet another generalization of Equation 3.1 with possible value in surface modelling. For two-dimensional curves generated in the x-y plane, they are equivalent.

3.1 The 2-D Superquadric Cylinder

In this section the equations related to the superquadric cylinder are given. The two-dimensional equation for the surface of the superquadric cylinder shown in Figure 3.1 is

$$f(X,Y)=\left|\frac{X}{a}\right|^{\nu}+\left|\frac{Y}{b}\right|^{\nu}=1. \tag{3.12}$$

As a parametric function of t where $-1 \le t \le +1$, the surface may be written as

$$\vec{r}(t)=X(t)\hat{x}+Y(t)\hat{y} \tag{3.13}$$

where

$$X(t)=\pm a\left(1-|t|^{\nu}\right)^{1/\nu}, \qquad Y(t)=bt. \tag{3.14}$$

The normal and tangent vectors to such a surface are

$$\hat{n}(X,Y)=\frac{\nabla f}{|\nabla f|}=\frac{\hat{x}b^{\nu}\,|X|^{(\nu-1)}\cdot\text{sign}\,(X)+\hat{y}a^{\nu}\,|Y|^{(\nu-1)}\cdot\text{sign}\,(Y)}{\sqrt{b^{2\nu}\,|X|^{2(\nu-1)}+a^{2\nu}\,|Y|^{2(\nu-1)}}} \tag{3.15}$$

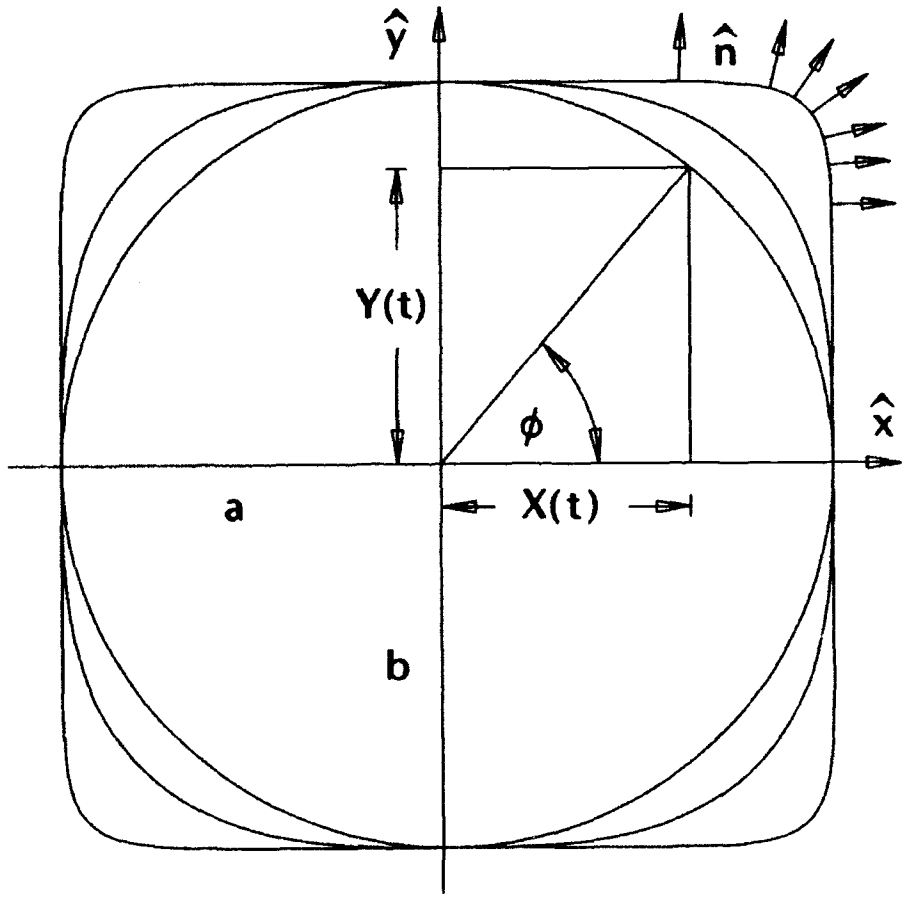

Figure 3.1: Various superellipses of $\nu = 2, 3, 10$.

$$\hat{t}(X,Y) = \hat{z} \times \hat{n} = \frac{-\hat{x}a^{\nu} |Y|^{(\nu-1)} \cdot \text{sign}\,(Y) + \hat{y}b^{\nu} |Y|^{(\nu-1)} \cdot \text{sign}\,(X)}{\sqrt{b^{2\nu} |X|^{2(\nu-1)} + a^{2\nu} |Y|^{2(\nu-1)}}} \tag{3.16}$$

so that

$$\vec{r}(t) = \pm\hat{x}a(1 - |t|^{\nu})^{1/\nu} + \hat{t}by \tag{3.17}$$

and

$$\hat{n}(t) = \frac{\pm\hat{x}b(1 - |t|^{\nu})^{(1-1/\nu)} + \hat{y}a\,|t|^{(\nu-1)}\,\text{sign}\,(t)}{\sqrt{b^2(1 - |t|^{\nu})^{2(1-1/\nu)} + a^2\,|t|^{2(\nu-1)}}} \tag{3.18}$$

Using the first angular parameterization,

$$\vec{r} = \hat{x}a\,|\cos v|^{(2/\nu)} \cdot \mathrm{sign}\,(\cos v) + \hat{y}b\,|\sin v|^{(2/\nu)} \cdot \mathrm{sign}\,(\sin v) \tag{3.19}$$

$$\hat{n}(v) = \frac{b\hat{x}\,|\cos v|^{(2-2/\nu)} \cdot \mathrm{sign}\,(\cos v) + a\hat{y}\,|\sin v|^{(2-2/\nu)} \cdot \mathrm{sign}\,(\sin v)}{\sqrt{b^2\,|\cos v|^{2(2-2/\nu)} + a^2\,|\sin v|^{2(2-2/\nu)}}}. \tag{3.20}$$

Note that the parameter v is not the same as the angle ϕ seen in Figure 3.1. The connection between the angle ϕ and parameter v is

$$v = \arctan\left[\left(\frac{a}{b}\tan\phi\right)^{(\nu/2)}\right] \tag{3.21}$$

$$\phi = \arctan\left[\frac{b}{a}\,(\tan v)^{(2/\nu)}\right]. \tag{3.22}$$

In the second angular parameterization, the relation between ψ and ϕ is

$$\psi = \arctan\left[\frac{a}{b}\tan\phi\right] \tag{3.23}$$

$$\phi = \arctan\left[\frac{b}{a}\tan\psi\right] \tag{3.24}$$

where

$$\vec{r}(\psi) = \frac{\hat{x}a\cos\psi + \hat{y}b\sin\psi}{\left(|\cos\psi|^{\nu} + |\sin\psi|^{\nu}\right)^{1/\nu}} \tag{3.25}$$

and

$$\hat{n}(\psi) = \frac{\hat{x}b\,|\cos\psi|^{\nu-1} \cdot \mathrm{sign}\,(\cos\psi) + \hat{y}a\,|\sin\psi|^{\nu-1} \cdot \mathrm{sign}\,(\sin\psi)}{\sqrt{b^2|\cos\psi|^{2(\nu-1)} + a^2\,|\sin\psi|^{2(\nu-1)}}}. \tag{3.26}$$

For a plane parametric curve of the form of Equation 3.13, the radius of curvature is given by

$$R_c(t) = \frac{\left[[X'(t)]^2 + [Y'(t)]^2\right]^{3/2}}{|X'(t)Y''(t) - Y'(t)X''(t)|}. \tag{3.27}$$

Thus the radius of curvature for the superquadric cylinder is

$$R_c(\phi) = \frac{(a^{2\nu}\sin\phi^{2\nu-2} + b^{2\nu}\cos\phi^{2\nu-2})^{(3/2)}}{(\nu-1)(ab)^{(\nu-1)}(\cos\phi\sin\phi)^{(\nu-2)}((a\sin\phi)^{\nu} + (b\cos\phi)^{\nu})^{(1+1/\nu)}}. \tag{3.28}$$

and

$$R_c(\psi) = \frac{(a^{2}\sin\psi^{2\nu-2} + b^{2}\cos\psi^{2\nu-2})^{(3/2)}}{ab(\nu-1)(\cos\psi\sin\psi)^{(\nu-2)}(\sin\psi^{\nu} + \cos\psi^{\nu})^{(1+1/\nu)}}. \tag{3.29}$$

Note that if ν equals anything other than exactly 2, the denominator of Equation 3.29 vanishes at $\phi = n\pi/2$, $n = 0, \pm 1, \pm 2$. Equation 3.29 is plotted in Figure 3.2. This is equivalent to a local zero in the curvature at the poles of the cylinder. The zero in curvature produces a "cusp" behavior at the poles seen in Figure 3.3. This cusp in curvature is the source of the singularity when using GO to calculate the reflected fields.

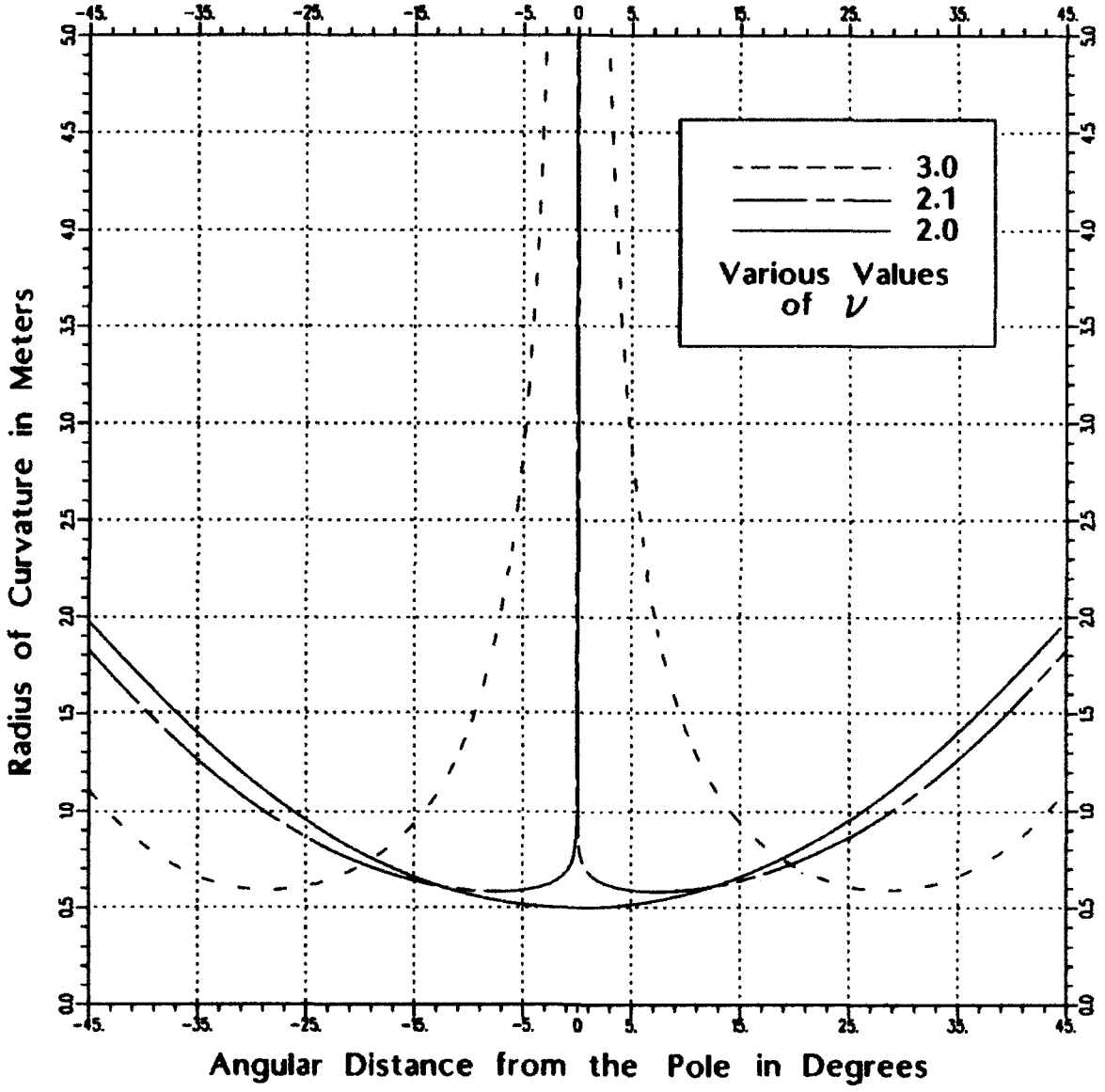

Figure 3.2: Superellipse radius of curvature $R_c(\psi)$ with $a = 2$ and $b = 1$.

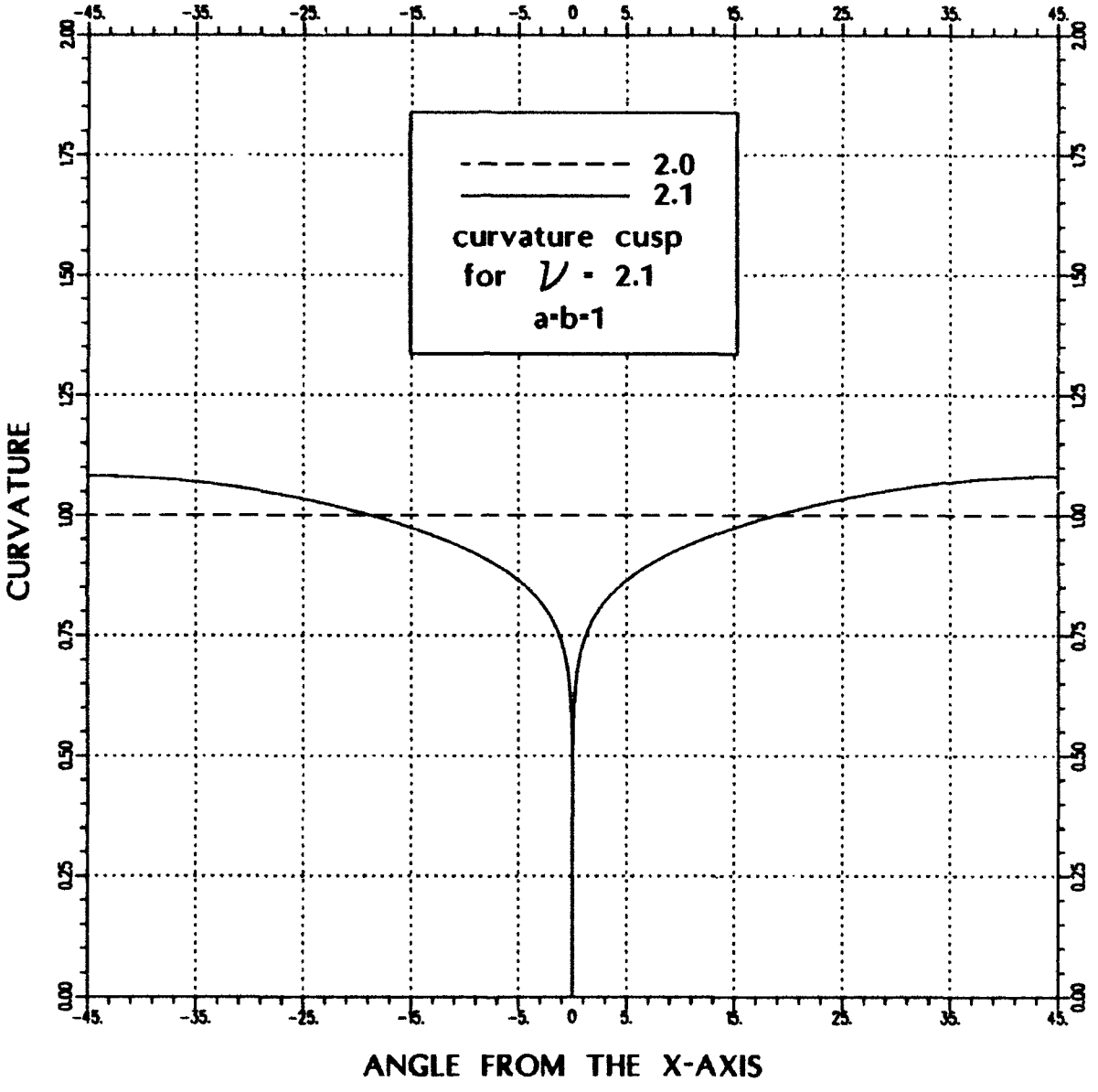

Figure 3.3: Superellipse curvature cusp with for $\nu = 2.0, 2.1$.

Chapter 4

GO AND PO SCATTERED FIELDS

This chapter presents the GO and PO formulations for the scattered fields from a superelliptic cylinder. By applying UTD concepts, the total scattering from the superellipse is seen to be composed of several mechanisms. As a minimum these include a reflected ray and a creeping wave around the back. Since the mechanism of interest here is the reflected ray, the other possible mechanisms are left as suggestions for further investigation.

4.1 The GO Reflected Field

For the superellipse geometry shown in Figure 2.1, the relevant parameters are

$$\phi = \arctan\left(\left|\frac{b^\nu}{a^\nu}\tan\left(\frac{\theta+\theta'}{2}\right)\right|^{\left(\frac{1}{\nu-1}\right)} \cdot \text{sign}\left[\tan\left(\frac{\theta+\theta'}{2}\right)\right]\right) \quad (4.1)$$

$$Q_r = ab\frac{[\hat{x}\cos\phi + \hat{y}\sin\phi]}{\left(|a\sin\phi|^\nu + |b\cos\phi|^\nu\right)^{1/\nu}} \quad (4.2)$$

$$E_z^i(Q_r) = E_o e^{-jks^i} \quad (4.3)$$

$$H_z^i(Q_r) = H_o e^{-jks^i} \tag{4.4}$$

$$R_c(Q_r) = \frac{(ab)^{(1-\nu)}(a^{2\nu}\sin\phi^{2\nu-2} + b^{2\nu}\cos\phi^{2\nu-2})^{(3/2)}}{(\nu-1)(\cos\phi\sin\phi)^{(\nu-2)}((a\sin\phi)^{\nu} + (b\cos\phi)^{\nu})^{(1+1/\nu)}} \tag{4.5}$$

$$\rho_c = \frac{1}{2}R_c(Q_r)\cos\theta^i \tag{4.6}$$

$$\hat{n} = \frac{\hat{x}b^{\nu}|\cos\phi|^{\nu-1}\cdot\mathrm{sign}(\cos\phi) + \hat{y}a^{\nu}|\sin\phi|^{\nu-1}\cdot\mathrm{sign}(\sin\phi)}{\sqrt{b^{2\nu}|\cos\phi|^{2(\nu-1)} + a^{2\nu}|\sin\phi|^{2(\nu-1)}}} \tag{4.7}$$

$$s^i = \rho' - \frac{ab\cos\theta^i}{(|a\sin\phi|^{\nu} + |b\cos\phi|^{\nu})^{1/\nu}} \tag{4.8}$$

$$s^r = \rho - \frac{ab\cos\theta^i}{(|a\sin\phi|^{\nu} + |b\cos\phi|^{\nu})^{1/\nu}} \tag{4.9}$$

$$\hat{\rho}' = \hat{x}\cos\theta' + \hat{y}\sin\theta' \tag{4.10}$$

$$\hat{\rho} = \hat{x}\cos\theta + \hat{y}\sin\theta \tag{4.11}$$

$$\hat{s}^i = -\hat{\rho}' \tag{4.12}$$

$$\hat{s}^r = \hat{\rho} \tag{4.13}$$

The far-field GO solution for $H_z^r(\vec{r})$ is therefore

$$H_z^r(\vec{r}) = H_o\sqrt{\rho_c}\frac{e^{-jk(r'+r)}}{\sqrt{r}}e^{jk2\cos\theta^i\frac{ab}{(|a\sin\phi|^{\nu}+|b\cos\phi|^{\nu})^{1/\nu}}} \tag{4.14}$$

with ϕ, $R_c(\phi)$ and θ^i given by Equations 4.1, 4.5 and 2.3. As is clear from the form of R_c (Equation 4.5, Figure 3.2), the solution produces infinite fields at the zero-curvature points of the superellipse. This is clearly a failure of GO. The full nature and reason for the failure is not clear from Equation 4.14, but becomes evident from Figure 3.2 when $\psi = (0, n\pi/2)$.

4.2 The PO Scattered Field

For an arbitrary 2-D surface, the PO formulation for the TE scattered field $\vec{H}^s$ is

$$\vec{H}^s = \sqrt{\frac{jk}{8\pi}} \frac{e^{-jk\rho}}{\sqrt{\rho}} \int_{C_{lit}} \left(\vec{J}_s(\vec{r}) \times \hat{s} \right) e^{jk(\vec{r}\cdot\hat{s})} \, d\ell \tag{4.15}$$

where

$$\begin{aligned}
\rho &= \text{Distance from the origin to the field point} \\
\vec{r} &= x\hat{x} + y\hat{y} \\
\hat{s} &= \hat{x}\cos\theta + \hat{y}\sin\theta \\
\vec{J}_s(\vec{r}') &= 2\hat{n} \times \vec{H}^i(\vec{r}) \\
\vec{H}^i(\vec{r}) &= \hat{z} e^{jk(\vec{r}\cdot\hat{s})} = \hat{z} e^{jk(x\cos\theta' + y\sin\theta')} \\
d\ell &= \text{Line integration element,}
\end{aligned}$$

as shown in Figure 4.1. Let the variable of integration be the parameter t. Then

$$\vec{r}(t) = \hat{x}a(1 - |t|^\nu)^{1/\nu} + \hat{y}bt \tag{4.16}$$

$$\vec{r} \cdot \hat{s} = a(1 - |t|^\nu)^{1/\nu} \cos\theta + bt \sin\theta \tag{4.17}$$

$$\hat{t}(t) = \frac{-\hat{x}a\,|t|^{(\nu-1)}\,\text{sign}\,(t) + \hat{y}b(1 - |t|^\nu)^{(1-1/\nu)}}{\sqrt{b^2(1 - |t|^\nu)^{2(1-1/\nu)} + a^2\,|t|^{2(\nu-1)}}} \tag{4.18}$$

$$\vec{J}_s(\vec{r}) \times \hat{s} = 2H_z^i(\vec{r})(\hat{n} \times \hat{z}) \times \hat{s} = -2H_z^i(\vec{r})(\hat{t} \times \hat{s}) \tag{4.19}$$

$$= 2\hat{z} e^{jk(x\cos\theta' + y\sin\theta')} \times \tag{4.20}$$

$$\times \frac{a\sin\theta\,|t|^{(\nu-1)}\,\text{sign}\,t + b\cos\theta(1 - |t|^\nu)^{(1-1/\nu)}}{\sqrt{b^2(1 - |t|^\nu)^{2(1-1/\nu)} + a^2\,|t|^{2(\nu-1)}}} \tag{4.21}$$

$$d\ell = \frac{\sqrt{a^2\,|t|^{2(\nu-1)} + b^2\,(1 - |t|^\nu)^{2(1-1/\nu)}}}{(1 - |t|^\nu)^{1-1/\nu}} \, dt. \tag{4.22}$$

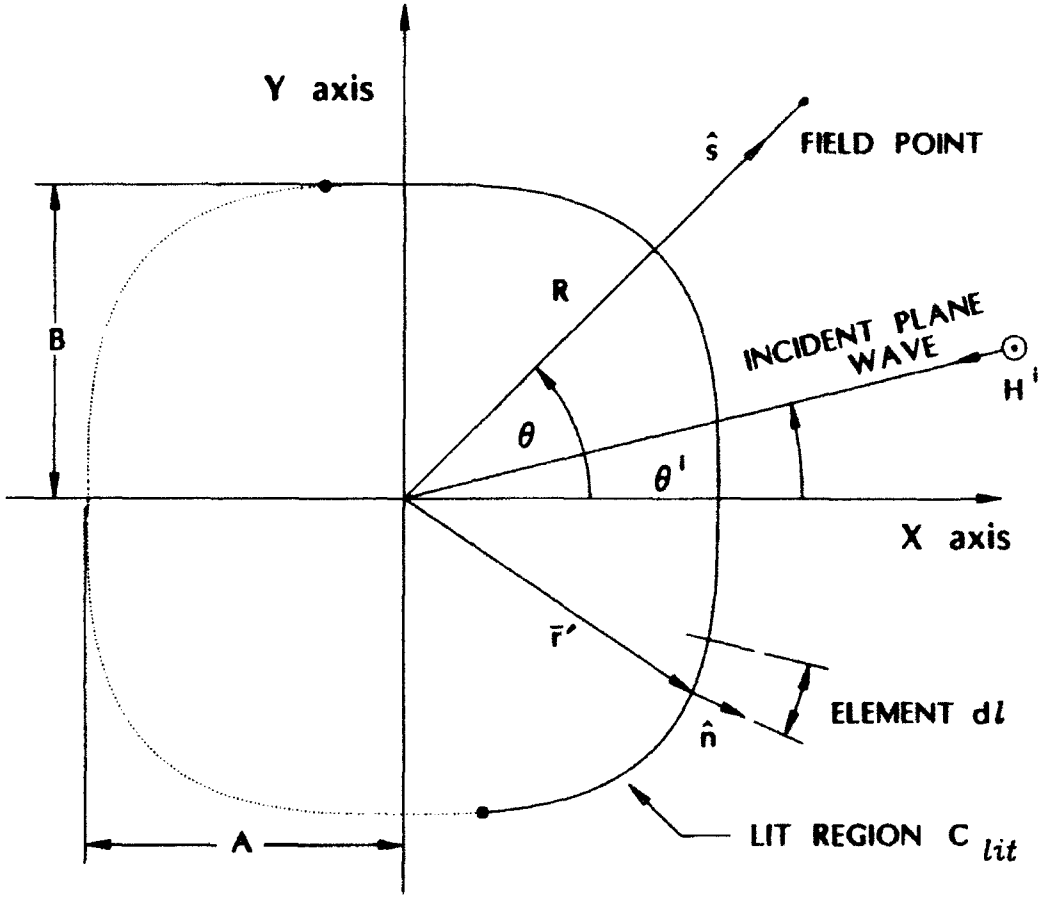

Figure 4.1: Geometry for the PO Scattered Field from the Superellipse

The PO integral for the scattered H_z^s field is then

$$H_z^s = \sqrt{\frac{jk}{2\pi}}\frac{e^{-jk\rho}}{\sqrt{\rho}}\int_{-1}^{+1}\left[a\frac{\sin\theta\,|t|^{\nu-1}\,\mathrm{sign}\,t}{(1-|t|^{\nu})^{(1-1/\nu)}}+b\cos\theta\right]\times$$
$$\times e^{jk\left(a(1-|t|^{\nu})^{1/\nu}(\cos\theta+\cos\theta')+bt(\sin\theta+\sin\theta')\right)}\,dt \qquad (4.23)$$

which may also be written as

$$H_z^s = \sqrt{\frac{jk}{2\pi}}\frac{e^{-jk\rho}}{\sqrt{\rho}}\int_0^1 \left\{\right.$$

$$
- \left[a \sin\theta \left(\frac{t}{(1-t^{\nu})^{(1/\nu)}} \right)^{(\nu-1)} - b\cos\theta \right] e^{jk\left(a(1-t^{\nu})^{1/\nu}(\cos\theta+\cos\theta')-bt(\sin\theta+\sin\theta')\right)}
$$

$$
+ \left[a \sin\theta \left(\frac{t}{(1-t^{\nu})^{(1/\nu)}} \right)^{(\nu-1)} + b\cos\theta \right] e^{jk\left(a(1-t^{\nu})^{1/\nu}(\cos\theta+\cos\theta')+bt(\sin\theta+\sin\theta')\right)}
$$

$$
\Bigg\} dt. \tag{4.24}
$$

Chapter 5

HIGH FREQUENCY ASYMPTOTIC EVALUATION OF THE PO INTEGRAL

5.1 Introduction

The Method of Steepest Descents is a general procedure for obtaining approximations to integrals with a large parameter k of the form

$$I(k) = \int_{\overline{P}} f(z) e^{kq(z)}\, dz. \tag{5.1}$$

The key to the approximation is that significant contributions to the integral will arise only from those parts of the path $\overline{P}$ that are local maxima (saddle points) of $\mathrm{Re}\{q(z)\}$ and the endpoints of $\overline{P}$. Contributions from the rest of the path will be exponentially smaller and may be neglected. The theory of steepest descent analysis is well developed and fully treated in [3,6].

A related method, the Method of Stationary Phase is applicable to integrals of the form

$$I(k) = \int_{x_1}^{x_2} f(x) e^{jkq(x)}\, dx \tag{5.2}$$

where again k is the large parameter. The method of stationary phase is based on the principle that rapidly fluctuating oscillatory functions tend to cancel under integration. Significant contributions to the integral will arise where there is a "stationary" point or a local cessation of oscillation. Note that while Equation 5.2 is a special case of Equation 5.1, the Method of Stationary Phase is *not* a special case of the Method of Steepest Descents. This is true because the contours of integration and the analyticity requirements are not the same for the two methods. Both methods yield the same result for the leading asymptotic term if the contour of one is continuously deformable into the contour of the other without encountering any singularities or branch points. A good discussion of the stationary phase method is found in [3,11].

5.2 Topology of the PO Integral

Although Equation 5.3 is a stationary phase integral, it will be evaluated by the method of steepest descents. The first step of an SDP analysis is to examine the structure of the integrand in the z-plane. Writing the stationary phase integral 4.24 in the form of Equation 5.1,

$$H_z^s = \sqrt{\frac{jk}{2\pi}} \frac{e^{-jk\rho}}{\sqrt{\rho}} \cdot I(k) \tag{5.3}$$

where

$$I(k) = I_1(k) + I_2(k) = \int_0^1 f_1(z) e^{kq_1(z)}\, dz + \int_0^1 f_2(z) e^{kq_2(z)}\, dz \qquad (5.4)$$

and

$$f_1(z) = -a\sin\theta \left(\frac{z}{(1-z^\nu)^{1/\nu}}\right)^{(\nu-1)} + b\cos\theta \qquad (5.5)$$

$$f_2(z) = +a\sin\theta \left(\frac{z}{(1-z^\nu)^{1/\nu}}\right)^{(\nu-1)} + b\cos\theta \qquad (5.6)$$

$$q_1(z) = j\left(a(1-z^\nu)^{1/\nu}(\cos\theta + \cos\theta') - bz(\sin\theta + \sin\theta')\right) \qquad (5.7)$$

$$q_2(z) = j\left(a(1-z^\nu)^{1/\nu}(\cos\theta + \cos\theta') + bz(\sin\theta + \sin\theta')\right). \qquad (5.8)$$

The structure of the integrands in Equation 5.4 is shown in Figure 5.1. The original contour of integration is along the positive real axis from 0 to 1. The functions $q_{1,2}(z)$ have branch points at the ν roots of unity located at

$$e^{j\frac{2n\pi}{\nu}}; \qquad n = 0, \pm 1, \pm 2 \cdots \nu. \qquad (5.9)$$

The associated branch cuts follow the contours of $\mathrm{Re}\{q(z)\} = 0$ so that subsequent contour deformations remain on the same Riemann sheet. In order to select the proper canonical integral, the behavior of $q(z)$ near the origin is of interest. The origin, in the z-plane, is where the multiple saddle points are situated. In the neighborhood of the origin,

$$q_{1,2}(z) \cong j\left(a(\cos\theta + \cos\theta')\left(1 - \frac{z^\nu}{\nu}\right) \mp bz(\sin\theta + \sin\theta')\right). \qquad (5.10)$$

For both I_1 and I_2, there will be $(\nu - 1)$ saddle points ($z_{s_{1j}}$ for I_1 and $z_{s_{2j}}$ for I_2, j=1,2,3 $\cdots \nu - 1$) that coalesce on the endpoint of integration at the origin. This is the primary contribution to the integral. The physical

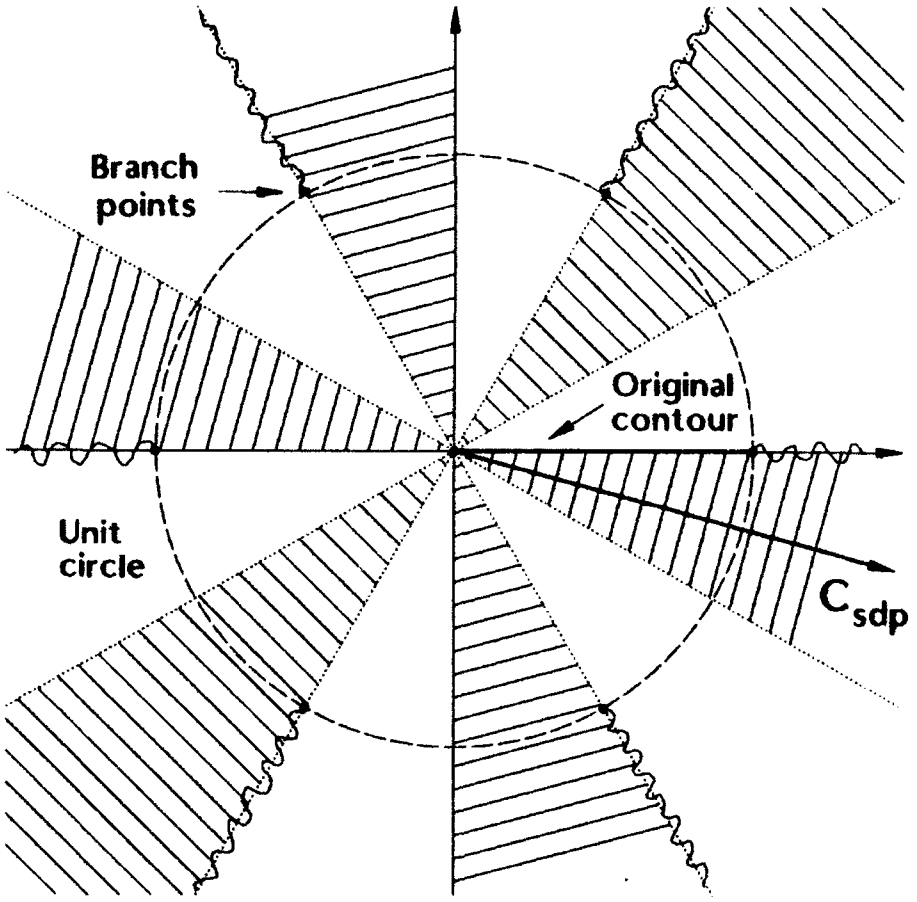

Figure 5.1: z-plane structure of q for $\nu = 6$.

meaning of the endpoint of $\overline{P}$ at $z = 1$ is a contribution due to the false termination currents of the PO approximation, and its effect on $I(k)$ will be ignored by deforming the original contour away from this point into the valley region shown in Figure 5.1.

5.3 Backscattered Field from the Curvature Cusp (the Pole)

For the special case of backscatter from the pole ($\theta = \theta' = 0$), Equations 5.3 through 5.8 simplify to

$$I(k) = 2I_1(k) = 2I_2(k) = 2\int_0^1 f_0(z)e^{kq_0(z)}\,dz \tag{5.11}$$

$$f_0(z) = b \tag{5.12}$$

$$q_0(z) = j2a(1-z^\nu)^{1/\nu}. \tag{5.13}$$

It is desired to approximate the structure of 5.13 near the saddle point $z_s = 0$ with a simplified exponential structure which can be integrated in closed form. In the neighborhood of the origin,

$$q_0(z) \cong 2ja\left(1-\frac{z^\nu}{\nu}\right). \tag{5.14}$$

For a transformation scheme, we have

$$I(k) = 2\int_0^1 f_0(z)e^{kq_0(z)}\,dz = 2b\int_0^1 e^{jk2a(1-z^\nu)^{1/\nu}}\,dz \tag{5.15}$$

$$\sim 2\int_0^\infty G_0(s)e^{k\tau_0(s)}\,ds = 2be^{jk2a}\int_0^\infty \left.\frac{dz}{ds}\right|_{s=0} e^{-ks^\nu}\,ds \tag{5.16}$$

where

$$G_0(s) = f(z)\frac{dz}{ds} \tag{5.17}$$

$$q_0(z) = \tau_0(s) = q_0(z_s) - s^\nu = j2a - s^\nu. \tag{5.18}$$

Equation 5.18 defines the transformation from the z-plane to the s-plane. The deformation of the contour from the upper limit of 1 in the z-plane to ∞ in the s-plane is justified on physical grounds. It causes the PO

termination currents to be excluded from the approximation. Expanding Equation 5.18 in a power series about $z_s = 0$,

$$q_0^{(\nu)}(z_s) = -2ja(\nu-1)! \tag{5.19}$$

$$\left.\frac{dz}{ds}\right|_{s=0} = e^{j\frac{2n\pi}{\nu}}\left[\frac{-\nu!}{q_0^{(\nu)}(z_s)}\right]^{1/\nu} \tag{5.20}$$

$$= e^{j\frac{2n\pi}{\nu}}\left[\frac{\nu}{2ja}\right]^{1/\nu} \tag{5.21}$$

where the choice of $n = 0, 1, 2 \cdots (\nu-1)$ is determined by the path leading away from z_s. From Figure 5.1 the appropriate choice for the arg of the steepest descent path is

$$\arg\left(\left.\frac{dz}{ds}\right|_{s=0}\right) = -\frac{\pi}{2\nu} \tag{5.22}$$

hence $n = 0$. The canonical integral used in Equation 5.15 is given in terms of the gamma function and is

$$\int_0^\infty e^{-ks^\nu}\,ds = \frac{1}{\nu k^{1/\nu}}\Gamma\left(\frac{1}{\nu}\right). \tag{5.23}$$

The resulting expression for $I(k)$ is

$$I(k) \sim 2\left[\frac{\nu}{2jka}\right]^{1/\nu} f(z_s)e^{kq_0(z_s)}\Gamma\left(\frac{1}{\nu}\right)\frac{1}{\nu} \tag{5.24}$$

$$= \frac{2b}{\nu}\Gamma\left(\frac{1}{\nu}\right)\left[\frac{\nu}{2ka}\right]^{1/\nu} e^{jk2a-j\frac{\pi}{2\nu}}. \tag{5.25}$$

The reflected field from the pole of a superellipse ($\theta = \theta' = 0$) given by Equation 5.3 becomes

$$H_z^s = \sqrt{\frac{jk}{2\pi}}\frac{2b}{\nu}\Gamma\left(\frac{1}{\nu}\right)\left[\frac{\nu}{2ka}\right]^{1/\nu}\frac{e^{-jk\rho}}{\sqrt{\rho}}e^{jk2a-j\frac{\pi}{2\nu}}. \tag{5.26}$$

When $\nu = 2$, the superellipse becomes a regular ellipse and Equation 5.26 reduces to

$$H_z^s = \sqrt{\frac{b^2}{2a}} \frac{e^{-jk\rho}}{\sqrt{\rho}} e^{jk2a} \tag{5.27}$$

which is the well-known result for the backscattered field from a 2-D elliptic cylinder. When $\nu \to \infty$, the superellipse becomes a box centered at the origin with width $2b$ and depth $2a$. In this case, Equation 5.26 reduces to

$$H_z^s = 2b\sqrt{\frac{jk}{2\pi}} \frac{e^{-jk\rho}}{\sqrt{\rho}} e^{jk2a} \tag{5.28}$$

which agrees with the PO result for the broadside backscatter from a strip of width $2b$ displaced along the x-axis by a. While the analysis is carried out for integer values of ν, comparison with numerical results shows that Equation 5.26 remains valid for all real values of ν between 2 and ∞.

5.4 Reflected Field Near and Far from the Pole for $\nu = 3$

The analysis for the case when $\nu = 3$ is based on the asymptotic expansion found in [7] which describes the arbitrary configuration of two simple saddle points situated near an integration end point. To find the saddle points we set the derivative of Equation 5.10 equal to zero. Then,

$$\frac{d}{dz}q_{1,2}(z) = j\left(-a\left(\cos\theta + \cos\theta'\right)\frac{z^2}{\left(1-z^3\right)^{2/3}} \mp b\left(\sin\theta + \sin\theta'\right)\right) = 0 \tag{5.29}$$

or for I_1,

$$\left[\frac{z_s}{\left(1-z_s{}^3\right)^{1/3}}\right]^2 = -\frac{b\left(\sin\theta + \sin\theta'\right)}{a\left(\cos\theta + \cos\theta'\right)} \tag{5.30}$$

and for I_2,

$$\left[\frac{z_s}{\left(1-z_s{}^3\right)^{1/3}}\right]^2 = +\frac{b\left(\sin\theta + \sin\theta'\right)}{a\left(\cos\theta + \cos\theta'\right)} \tag{5.31}$$

so that the saddle points for I_1 are located at

$$z_{11} = -\left[\frac{\left[b\sin\left(\frac{\theta+\theta'}{2}\right)\right]^{3/2}}{j\left[a\cos\left(\frac{\theta+\theta'}{2}\right)\right]^{3/2} - \left[b\sin\left(\frac{\theta+\theta'}{2}\right)\right]^{3/2}}\right]^{1/3} \tag{5.32}$$

$$z_{12} = +\left[\frac{\left[b\sin\left(\frac{\theta+\theta'}{2}\right)\right]^{3/2}}{j\left[a\cos\left(\frac{\theta+\theta'}{2}\right)\right]^{3/2} + \left[b\sin\left(\frac{\theta+\theta'}{2}\right)\right]^{3/2}}\right]^{1/3} \tag{5.33}$$

and those for I_2 are located at

$$z_{21} = -\left[\frac{\left[b\sin\left(\frac{\theta+\theta'}{2}\right)\right]^{3/2}}{\left[a\cos\left(\frac{\theta+\theta'}{2}\right)\right]^{3/2} - \left[b\sin\left(\frac{\theta+\theta'}{2}\right)\right]^{3/2}}\right]^{1/3} \tag{5.34}$$

$$z_{22} = +\left[\frac{\left[b\sin\left(\frac{\theta+\theta'}{2}\right)\right]^{3/2}}{\left[a\cos\left(\frac{\theta+\theta'}{2}\right)\right]^{3/2} + \left[b\sin\left(\frac{\theta+\theta'}{2}\right)\right]^{3/2}}\right]^{1/3}. \tag{5.35}$$

The asymmetry in the saddle point locations would cause great complications in the analysis. For relatively small values of $(\theta + \theta')/2$, however, the saddle points may be approximated by

$$z_s = \left[\frac{\left[b \sin\left(\frac{\theta+\theta'}{2}\right)\right]^{3/2}}{\left[a \cos\left(\frac{\theta+\theta'}{2}\right)\right]^{3/2} + \left[b \sin\left(\frac{\theta+\theta'}{2}\right)\right]^{3/2}} \right]^{1/3} \tag{5.36}$$

$$z_{11} = +j\,|z_s| \tag{5.37}$$

$$z_{12} = -j\,|z_s| \tag{5.38}$$

$$z_{21} = -\,|z_s| \tag{5.39}$$

$$z_{22} = +\,|z_s|\,. \tag{5.40}$$

For larger θ, θ', the saddle points are widely separated and the inaccuracy of the above assumption diminishes exponentially. Because of symmetry of Equations 5.37 through 5.40, the following relations hold true.

$$f_1(z_{11}) = f_1(z_{12}) = f_2(z_{21}) = f_2(z_{22}) \tag{5.41}$$

$$= b\cos\theta + a\sin\theta \left(\frac{z_s}{(1 - {z_s}^3)^{(1/3)}} \right)^2 \tag{5.42}$$

$$q_2''(z_{21}) = -q_2''(z_{22}) = jq_1''(z_{11}) = -jq_1''(z_{12}) \tag{5.43}$$

$$= 2ja(\cos\theta + \cos\theta') \left(\frac{z_s}{(1 - {z_s}^3)^{(5/3)}} \right). \tag{5.44}$$

The integrals I_1 and I_2 are treated separately, though the strategy of analysis is the same for both. If

$$I_r(k) = \int_{z_{ra}}^{\infty_r} f_r(z) e^{kq_r(z)}\, dz = \int_{s_{ra}}^{\infty_r} G_r(s) e^{k\tau_r(s)}\, ds \qquad r = 1, 2 \tag{5.45}$$

where the functions $q_r(z)$ have two first-order saddle points at $z_{r1,r2}$ then the asymptotic expansion of $I_r(k)$ valid uniformly as $z_{r1} \to z_{r2} \to z_{ra}$ and

as $k \to \infty$ is given [7] by

$$
\begin{aligned}
I_r(k) \;\sim\; & \pi\left[H_r(s_{r1}) + H_r(s_{r2})\right] \frac{e^{ka_{r0}}}{k^{1/3}} G_{ri}(s_{r1}^2 k^{2/3}, k^{1/3} s_{ra}) \\
+ \; & \pi\left[H_r(s_{r1}) - H_r(s_{r2})\right] \frac{e^{ka_{r0}}}{k^{2/3} s_{r1}} G'_{ri}(s_{r1}^2 k^{2/3}, k^{1/3} s_{ra}) \\
- \; & \left[H_r(s_{ra}) - \left(1 + \frac{s_{ra}}{s_{r1}}\right) \frac{H_r(s_{r1})}{2} - \left(1 - \frac{s_{ra}}{s_{r1}}\right) \frac{H_r(s_{r2})}{2}\right] \times \\
& \times \frac{e^{k\tau_r(s_{ra})}}{k(s_{r1}^2 - s_{ra}^2)} \qquad r = 1, 2
\end{aligned} \tag{5.46}
$$

where the transformation from the z-plane to the s-plane is

$$q_r(z) = \tau_r(s) = a_{r0} + s\eta_r - \frac{s^3}{3} \tag{5.47}$$

$$q_r(z_{ra}) = \tau_r(s_{ra}) \tag{5.48}$$

$$a_{r0} = \frac{1}{2}\left[q_r(z_1) + q_r(z_2)\right] \tag{5.49}$$

$$\sqrt{\eta_r} = \left[\frac{3}{4}\left(q_r(z_1) - q_r(z_2)\right)\right]^{1/3} \equiv s_{r1} = -s_{r2} \tag{5.50}$$

and

$$H_r(s) = f_r(z)\frac{dz}{ds} \tag{5.51}$$

$$\left.\frac{dz}{ds}\right|_{s_{r1}, s_{r2}} = \sqrt{\frac{\mp 2 s_{r1}}{q''(z_{r1,r2})}} \equiv h_{r1,r2} \tag{5.52}$$

$$\left.\frac{dz}{ds}\right|_{s_{ra}} = \frac{s_{r1}^2 - s_{ra}^2}{q'(z_{ra})} \tag{5.53}$$

$$G_{ri}(\xi, \beta) = \frac{1}{2\pi j} \int_{\beta_{ri}}^{\text{"}\infty_r\text{"}} e^{\xi t - t^3/3}\, dt \tag{5.54}$$

$$G'_{ri}(\xi, \beta) = \frac{G_{ri}(\xi, \beta)}{d\xi}. \tag{5.55}$$

The function G_i is expressible in terms of the Incomplete Airy Functions given in Appendix A. To apply this approximation to I_1, the proper branch of $\sqrt{\eta_1}$ must be selected. This means first choosing m such that

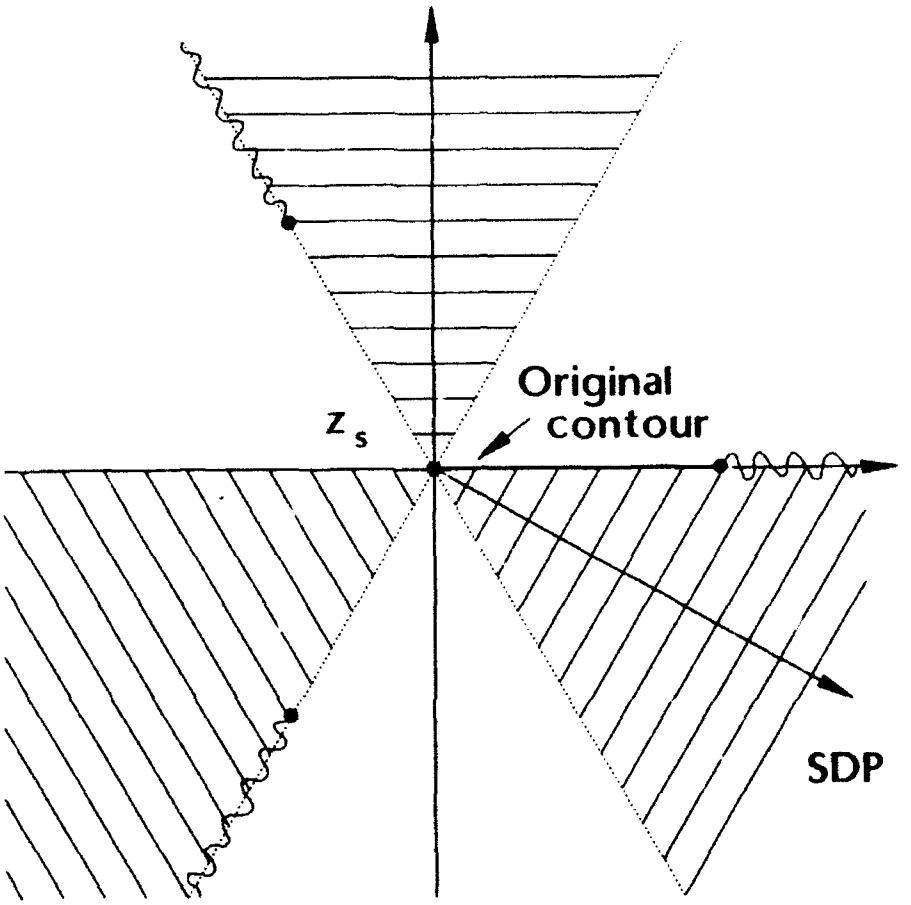

Figure 5.2: Map of $\mathrm{Re}[q_{1,2}(z)]$ for $z_{11} = z_{12} = z_s$.

$$\left.\frac{dz}{ds}\right|_{s=0} = \left[\frac{-2}{q_1'''(z_s)}\right]^{1/3} = \left|\frac{2}{q_1'''(z_s)}\right|^{1/3} e^{-j\frac{\pi}{6}+j\frac{2m\pi}{3}}; \qquad m = 0, \pm 1, \pm 2 \quad (5.56)$$

agrees with the arg of the SDP of Figure 5.2. The indicated choice is $m = 0$ so that $\arg(h_{11})|_{s=0}$ must equal $-\frac{\pi}{6}$. This then determines the choice of branch for $\sqrt{\eta_1}$ since it must be consistent with Equation 5.52. Then

$$h_{11} = \left|\frac{2\eta_1^{1/2}}{q''(z_{11})}\right|^{1/2} e^{j\frac{\pi}{3}+j\frac{2n\pi}{6}}; \qquad n = 0, \pm 1, \pm 2 \qquad (5.57)$$

so that

$$e^{-j\frac{\pi}{6}} = e^{+j\frac{\pi}{6}(3-2n)}. \tag{5.58}$$

This equation is satisfied for $n = 2$ so that

$$\eta_1^{1/2} = |\eta_1|^{1/2} e^{+j\frac{2\pi}{3}} \tag{5.59}$$

$$\eta_1 = |\eta_1| e^{-j\frac{2\pi}{3}} \tag{5.60}$$

$$h_{11} = h_{12} = \left| \frac{2\eta_1^{1/2}}{q''(z_{11})} \right|^{1/2} e^{-j\frac{\pi}{6}}. \tag{5.61}$$

From Equations 5.37, 5.38 and 5.48, $s_{ra} \approx 0$ and using A.28, A.31 and A.37 Equation 5.46 becomes

$$\begin{aligned} I_1(k) \sim\ & \pi \left[f_1(z_{11})h_{11} + f_1(z_{12})h_{12} \right] \frac{e^{ka_0}}{k^{1/3}} e^{j\frac{\pi}{6}} G_1^* \left(|\eta_1| k^{2/3}, 0 \right) \\ +\ & \pi \left[f_1(z_{11})h_{11} - f_1(z_{12})h_{12} \right] \frac{e^{ka_0}}{k^{1/3}\eta_1^{1/2}} e^{-j\frac{5\pi}{12}} G_1'^* \left(|\eta_1| k^{2/3}, 0 \right) \\ +\ & \frac{e^{kq_1(0)}}{k} \left[\frac{f_1(z_{11})h_{11} + f_1(z_{12})h_{12}}{2\eta_1} - \frac{f_1(0)}{q_1'(0)} \right]. \end{aligned} \tag{5.62}$$

Substituting Equations 5.37 through 5.40 into Equations 5.5 through 5.8 and making use of Equation 5.61, Equation 5.62 reduces to

$$\begin{aligned} I_1(k) \sim\ & 2\pi f_1(z_{11})h_{11} \frac{e^{ka_0}}{k^{1/3}} e^{j\frac{\pi}{6}} G_1^* \left(|\eta_1| k^{2/3}, 0 \right) \\ +\ & \frac{e^{kq_1(0)}}{k} \left[\frac{f_1(z_{11})h_{11}}{\eta_1} - \frac{f_1(0)}{q_1'(0)} \right]. \end{aligned} \tag{5.63}$$

When $\eta \neq 0$, the saddle points for I_1 are situated as shown in Figure 5.3.

Turning attention now to I_2, the proper choice of $\arg(\sqrt{\eta_2})$ must again be made and m must be selected so that

$$\left. \frac{dz}{ds} \right|_{s=0} = \left[\frac{-2}{q_1'''(z_s)} \right]^{1/3} = \left| \frac{2}{q_1'''(z_s)} \right|^{1/3} e^{-j\frac{\pi}{6} + j\frac{2m\pi}{3}}; \qquad m = 0, \pm 1, \pm 2 \tag{5.64}$$

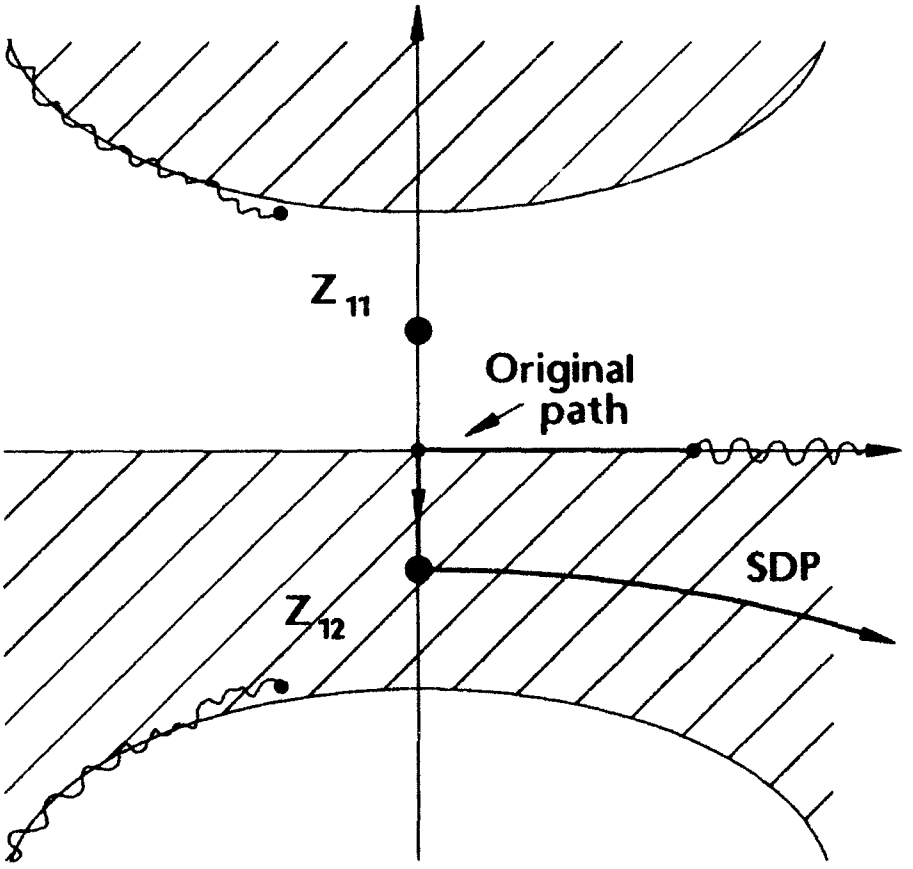

Figure 5.3: Contours of Integration and Map of $\mathrm{Re}[q_1(z)]$ for $z_{11} \neq z_{12}$.

agrees with the arg of the SDP of Figure 5.4. The indicated choice is $m = 0$ so that $\arg(h_{21})|_{s=0} = -\frac{\pi}{6}$. The choice of branch for $\sqrt{\eta_1}$ is then

$$h_{21} = \left| \frac{2\eta_2^{1/2}}{q''(z_{21})} \right|^{1/2} e^{j\frac{\pi}{4} - j\frac{\pi}{12} + j2n\pi}; \qquad n = 0, \pm 1, \pm 2 \tag{5.65}$$

so that

$$e^{-j\frac{\pi}{6}} = e^{+j\frac{\pi}{6}(1+2n)}. \tag{5.66}$$

This equation is satisfied for $n = -1$ so that

$$\eta_2^{1/2} = |\eta_2|^{1/2} e^{-j\frac{3\pi}{6}} \tag{5.67}$$

$$\eta_2 = -|\eta_2| e^{-j\frac{2\pi}{3}} \tag{5.68}$$

$$h_{21} = h_{22} = \left| \frac{2\eta_2^{1/2}}{q''(z_{21})} \right|^{1/2} e^{-j\frac{\pi}{6}}. \tag{5.69}$$

This results in

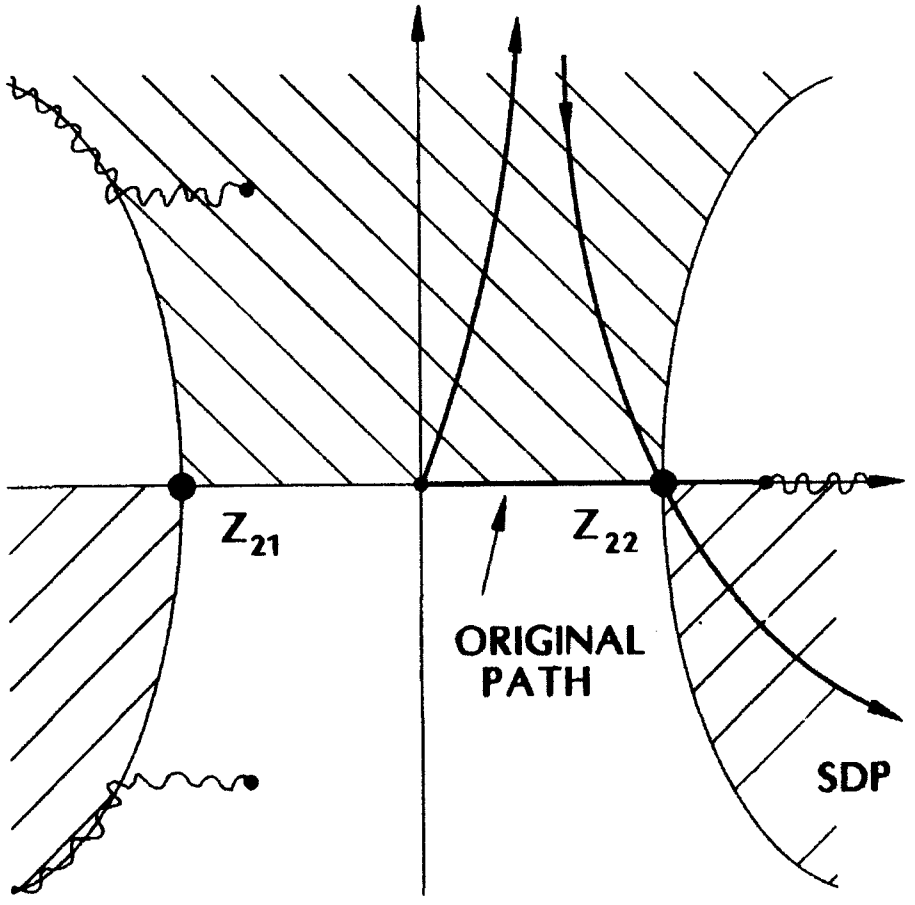

Figure 5.4: Contours of Integration and Map of Re$[q_2(z)]$

$$
\begin{aligned}
I_2(k) \;\sim\; & \pi\left[f_2(z_{21})h_{21} + f_2(z_{22})h_{22}\right]\frac{e^{ka_0}}{k^{1/3}}e^{j\frac{\pi}{6}}G_1^*\left(-|\eta_2|\,k^{2/3},0\right) \\
+\; & \pi\left[f_2(z_{21})h_{21} - f_2(z_{22})h_{22}\right]\frac{e^{ka_0}}{k^{1/3}\eta_2^{1/2}}e^{-j\frac{5\pi}{12}}G_1'^*\left(-|\eta_2|\,k^{2/3},0\right) \\
+\; & \frac{e^{kq_2(0)}}{k}\left[\frac{f_2(z_{21})h_{21} + f_2(z_{22})h_{22}}{2\eta_2} - \frac{f_2(0)}{q_2'(0)}\right]. \qquad (5.70)
\end{aligned}
$$

which using Equations 5.37 through 5.40 and Equations 5.5 through 5.8 and 5.69 simplifies to

$$
\begin{aligned}
I_2(k) \;\sim\; & 2\pi f_2(z_{21})h_{21}\frac{e^{ka_0}}{k^{1/3}}e^{j\frac{\pi}{6}}G_1^*\left(-|\eta_2|\,k^{2/3},0\right) \\
+\; & \frac{e^{kq_2(0)}}{k}\left[\frac{f_2(z_{21})h_{21}}{\eta_2} - \frac{f_2(0)}{q_2'(0)}\right]. \qquad (5.71)
\end{aligned}
$$

Forming the sum of I_1 and I_2 leads to further simplifications. Using

$$
\begin{aligned}
q_1(0) &= q_2(0) && (5.72)\\
q_1'(0) &= -q_2'(0) && (5.73)\\
\eta_1 &= -\eta_2 && (5.74)\\
h_{11} &= h_{21} && (5.75)
\end{aligned}
$$

with Equation 5.41 results in

$$
\begin{aligned}
I(k) &= I_1(k) + I_2(k) \\
&\sim 2\pi f_2(z_{22})h_{22}\frac{e^{ka_0}}{k^{1/3}}e^{j\frac{\pi}{6}} \times \\
&\quad \times\left[G_1^*\left(+|\eta_2|\,k^{2/3},0\right) + G_1^*\left(-|\eta_2|\,k^{2/3},0\right)\right] \qquad (5.76)
\end{aligned}
$$

or

$$
\begin{aligned}
I(k) \;\sim\; & 2\pi f_2(z_s)\left|\frac{2\eta_2^{1/2}}{k^{2/3}q''(z_s)}\right|^{1/2} e^{k\frac{1}{2}(q_2(z_s)+q_2(z_s))} \times \\
& \times\left[G_1^*\left(+|\eta_2|\,k^{2/3},0\right) + G_1^*\left(-|\eta_2|\,k^{2/3},0\right)\right]. \qquad (5.77)
\end{aligned}
$$

While Equation 5.77 is complete, it is not in the best form for comparison to the (singular) first-order stationary phase result. By rearranging the solution so that the first-order stationary phase solution is a visible factor, insight may be gained about the nature of the corrected solution. The usual first order isolated saddle-point solution for this cylinder is

$$I(k) \sim f(z_s)\sqrt{\frac{2\pi}{k\,|q''(z_s)|}}e^{jk|q(z_s)|-j\frac{\pi}{4}}. \tag{5.78}$$

Using Equation 5.49, Equation 5.77 may be rewritten as

$$I(k) \sim \left[f_2(z_s)\sqrt{\frac{2\pi}{k\left|q_2''(z_s)\right|}}e^{jk|q_2(z_s)|-j\frac{\pi}{4}}\right] \times T(\eta k^{2/3}) \tag{5.79}$$

where

$$T(x) = \left[2\sqrt{\pi}e^{j\frac{\pi}{4}}\,|x|^{1/4}\,e^{-j\frac{2}{3}|x|^{3/2}}\left(\overline{\mathrm{Ai}}^{*}(+|x|,0)+\overline{\mathrm{Ai}}^{*}(-|x|,0)\right)\right] \tag{5.80}$$

$$\eta = \left[\frac{3}{4}\,|q_2(+z_s)-q_2(-z_s)|\right]^{2/3} \tag{5.81}$$

and the Airy Functions are as described in Appendix A.

From the above equations, it is seen that the analysis for the two first-order coalescing saddle points results in a form that can be written as the first-order stationary phase evaluation multiplied by a function T. This function acts as a correction to the singular first-order result. Functions of this kind in UTD are called Transition Functions. Since it is known that the GO result agrees with the first-order stationary phase evaluation for the reflected field far away from the pole, it is anticipated that the transition function $T(x)$ is the desired multiplicative correction to GO. The expected behavior of the transition function $T(x)$ then for large argument

is magnitude of unity and a phase of zero. This is seen in Figure 5.5. For small argument x, $T(x)$ should approach zero in such a way that the product of $T(x)$ and the infinite GO term result in a finite and accurate limiting value for the field at the pole. The large argument form of the Incomplete Airy Function is given in Appendix A. Thus for $x \gg 0$,

$$\begin{aligned} T(x) &\sim \left[2\sqrt{\pi}e^{j\frac{\pi}{4}}|x|^{1/4}e^{-j\frac{2}{3}|x|^{3/2}}\left(\left(\frac{1}{2\pi jx}\right)+\left(\frac{-1}{2\pi jx}+\frac{1}{2\pi}\sqrt{\frac{\pi}{jx^{1/2}}}e^{j\frac{2}{3}|x|^{3/2}}\right)\right)\right] \\ &= 1. \end{aligned} \tag{5.82}$$

For $x \approx 0$,

$$\begin{aligned} T(x) &\approx 2\sqrt{\pi}e^{j\frac{\pi}{4}}|x|^{1/4}\left(\frac{e^{-j\pi/6}}{2\pi}\Gamma(\frac{1}{3})\frac{1}{3^{2/3}}+\frac{e^{-j\pi/6}}{2\pi}\Gamma(\frac{1}{3})\frac{1}{3^{2/3}}\right) \\ &= \frac{2}{3^{2/3}}\frac{\Gamma(\frac{1}{3})}{\sqrt{\pi}}e^{j\frac{\pi}{12}}|x|^{1/4} \approx 1.453e^{j\pi/12}|x|^{1/4} \end{aligned} \tag{5.83}$$

For $(\theta+\theta') \approx 0$, Equations 4.1 and 4.5 show that the order of the singularity of $\sqrt{\rho_c}$ is

$$\sqrt{\rho_c} \propto [\theta+\theta']^{\left(-\frac{\nu-2}{2\nu-2}\right)}. \tag{5.84}$$

For $\nu = 3$, this is $O(x^{-1/4})$. The behavior of η for $(\theta+\theta') \approx 0$ is $\eta \propto [\theta+\theta']$. Then the behavior of $T(\eta k^{2/3})$ is

$$T(\eta k^{2/3}) \propto [\theta+\theta']^{1/4}. \tag{5.85}$$

Since this is a zero of order $O(x^{+1/4})$, then the GO singularity is indeed cancelled.

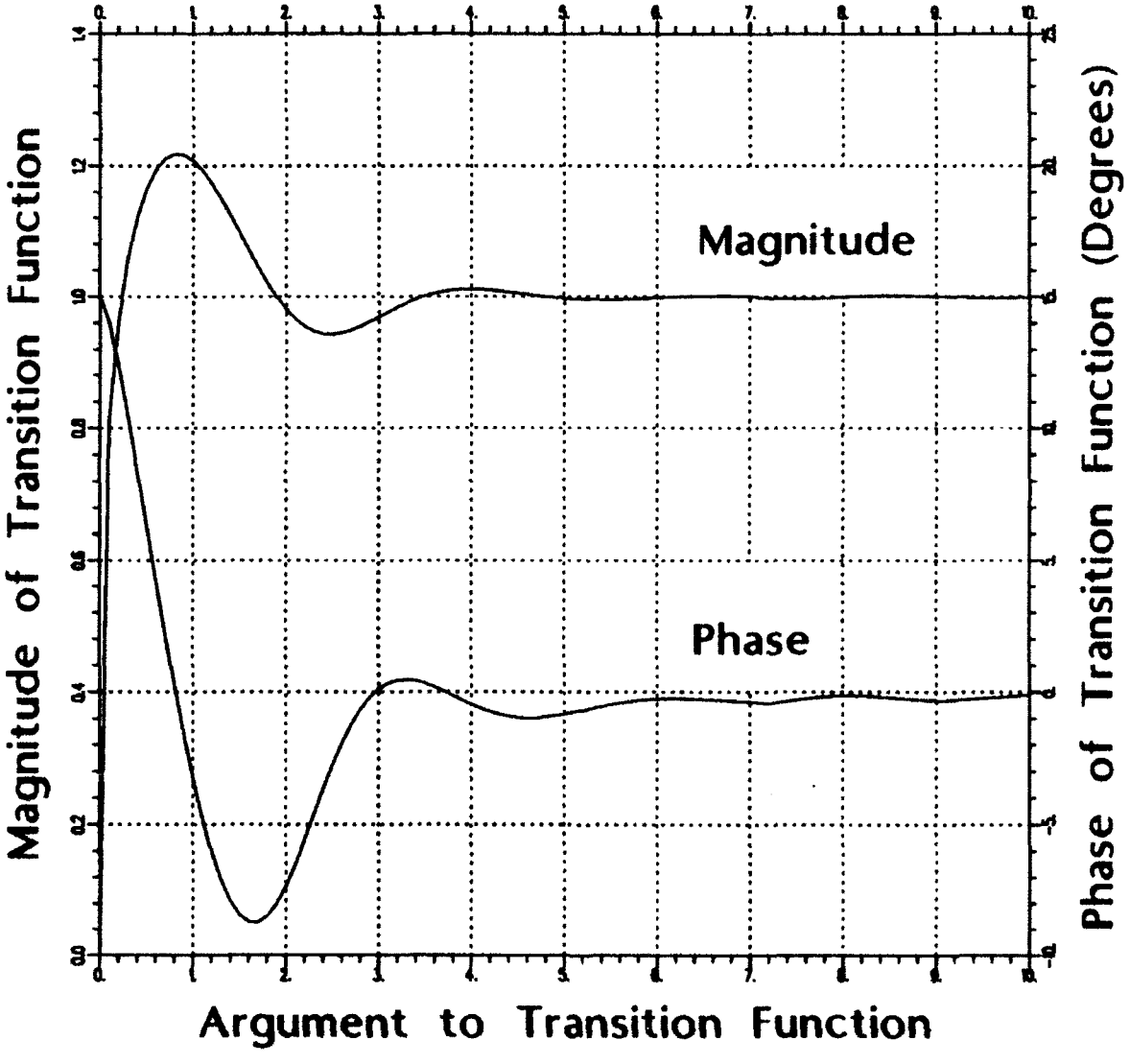

Figure 5.5: The Transition Function $T(x)$.

5.5 The Uniform GO (UGO) Solution for $\nu = 3$

The total corrected GO expression for the reflected field from a superelliptic cylider with $\nu = 3$ is then

$$H_z^r(\vec{\rho}) = H_o\sqrt{\rho_c}\frac{e^{-jk(\rho'+\rho)}}{\sqrt{\rho}}e^{jk2\cos\theta^i\frac{ab}{(|a\sin\phi|^\nu+|b\cos\phi|^\nu)^{1/\nu}}} \times T(\eta k^{2/3}) \qquad (5.86)$$

where, using Equations 5.81, 5.10 and 5.36,

$$\eta \cong b\sin\left(\frac{\theta+\theta'}{2}\right)\left[\frac{2\cos\left(\frac{\theta-\theta'}{2}\right)}{\left(\left(a\cos\left(\frac{\theta+\theta'}{2}\right)\right)^{3/2}+\left(b\sin\left(\frac{\theta+\theta'}{2}\right)\right)^{3/2}\right)^{1/3}}\right]^{2/3} \qquad (5.87)$$

and ϕ, θ^i, ρ_c and $T(x)$ are given by Equations 4.1, 2.3, 4.6 and 5.80.

For small $(\theta+\theta')/2$, η behaves like

$$\eta \simeq 2^{2/3}\frac{b}{a}\tan\left(\frac{\theta+\theta'}{2}\right). \qquad (5.88)$$

The angular region where the pure GO result is invalid may be determined via Equation 5.87. When $\eta k^{2/3} > 10$, then $T(\eta k^{2/3}) \sim 1$. When $\eta k^{2/3} < 3.5$, then $T(\eta k^{2/3})$ begins to make significant corrections to the GO result. A subjective criterion for a significant departure from the GO result (resulting in a greater than .04 dB deviation) is $\eta k^{2/3} < 5$.

The numerical results UGO, GO, PO, and the Method of Moments are presented in Chapter 6.

5.6 Reflected Field Behavior for $\nu \neq 3$

The correction to the GO solution takes the form of a two-parameter multiplicative transition function $T(x,\nu)$ where ν is the superelliptic "square-

ness" parameter, and x is a variable describing the proximity of the reflection point to the pole, or zero-curvature point. The transition function $T(x,\nu)$ does two things near the pole; it acts to correct the GO singularity, and it furnishes an aperture-like oscillatory pattern behavior. As ν gets large and the surface around the pole flattens, this aperture effect becomes more and more pronounced. In the limit of infinite ν, a $\left[\frac{\sin x}{x}\right]$ type of pattern is expected.

The results of Chapter 5 explored two aspects of $T(x,\nu)$. First, the limiting case of $H_{g_0} \cdot T(x=0,\nu)$ is examined. This result is expressed in terms of the Gamma Function and corresponds to an evaluation of the field reflected from the pole itself for arbitrary ν. Second, $T(x,\nu=3)$ is expressed in terms of Incomplete Airy Functions. $T(x,\nu=3)$ is associated with the reflected field both near and far from the pole, but only for the superellipse whose $\nu=3$.

The general function $T(x,\nu)$ cannot be expressed in terms of known functions, but it is hypothesized that the general transition function accounting for the distributed current effects around the pole may be constructed heuristically, based on a generalization of the integral form of the Incomplete Airy Function, i.e.

$$F(\eta,\nu) = \int_0^\infty \left(e^{+j\eta t} + e^{-j\eta t}\right) e^{j\frac{t^\nu}{\nu}}\, dt \tag{5.89}$$

$$= 2\int_0^\infty \cos(\eta t) e^{j\frac{t^\nu}{\nu}}\, dt. \tag{5.90}$$

The full steepest-descent-path analysis is not tractable for the general case of N merging saddle points. In spite of this, there is reason to believe that Equation 5.90 may form the basis for a workable $T(x,\nu)$ after all.

A comparison of the kernels of Equations 4.24, 5.10 and 5.90 reveal that their structures are the same in the neighborhood of $t = 0$ for all ν. It is not therefore unreasonable to suggest that Equation 5.90 is in fact the correct canonical form on which to base the general correction $T(x, \nu)$. Further, because the integration increment dt is strictly a real quantity, Equation 5.90 easily generalizes to all real ν. The question therefore is whether Equation 5.90 is sufficiently characteristic of superellipse behavior to construct a simple and accurate $T(x, \nu)$, or whether other complicating factors arise.

As ν becomes large, another effect appears, which is quite unrelated to the difficulties associated with the pole. The regions where the radius of curvature decreases with increasing ν develop into sharp corners. In these regions, GO is valid provided that the smallest radius of curvature is much larger than the wavelength. A natural transition from the mechanism of reflection over to diffraction must be incorporated into the solution to achieve full generality for large ν on electrically small cylinders. Some pertinent results concerning reflection by surfaces with electrically small radii of curvature are found in [4].

Chapter 6

NUMERICAL RESULTS

This chapter presents the numerical data for the reflected field from various superelliptic cylinders, calculated by the various methods of GO, UGO, PO, and MoM. First, results for reflection from the pole are presented, then results for reflection near and far from the pole for $\nu = 3$ cylinders are presented. The curves display the different scattering mechanisms and/or artifacts contained in the various methods. Whenever possible, an interpretation of the results will be pointed out in the discussions accompanying the graphs.

With regard to efficiency, it is worth noting that in Table 6.1, the UGO

	a=b=1λ	a=b=3λ	a=b=5λ	a=b=10λ	a=b=30λ
GO	.88 s	.83 s	.77 s	.72 s	.83 s
UGO	31.4 s	16.9 s	12.4 s	8.25 s	5.1 s
PO	36.1 s	1.8 min.	3.2 min.	6.0 min.	18 min.
MoM	1.7 min.	4.8 min.	9.5 min.	32 min.	> 4 hrs.

Table 6.1: Comparative CPU times in VPU (VAX 780 Processing Units)

solution for electrically large cylinders is more than two orders of magnitude faster than Physical Optics, and more than three orders of magnitude faster than the Method of Moments. Further, the UGO solution is the only method whose computation time *decreases* as the scatterer gets larger. This phenomenon is due to the asymptotic behavior of the transition function $T(x, \nu = 3)$; it is easier to compute for large arguments. While GO is also very efficient, it does not produce a uniformly valid result around the pole.

The slight variations visible in the GO CPU times reflect the variabilities and inefficiencies which exist in a multiuser computer environment. The actual computations were performed on a VAX 8550 running the VMS operating system. Each entry in Table 6.1 represents 90 backscattered field computations for a $\nu = 3$ superquadric cylinder.

6.1 Reflected Fields from the Pole for Arbitrary ν

The basic asymptotic result concerning the backscattered field from the pole is given by Equation 5.26. This equation is a Physical Optics approximation of the reflected field from the pole, neglecting the second-order effect of creeping waves, and excluding false PO current terminations. The backscatter field for various types of superellipsoids is plotted versus ν in Figure 6.1. Should future research produce a general reflection transition function $T(x, \nu)$, Equation 5.26 will be useful as a check on the small argument x limit of $T(x, \nu)$, since 5.26 is valid for all ν.

Figure 6.1 illustrates that the UGO solution provides a smooth tran-

sition from ($\sqrt{a/2}$) type of behavior which is characteristic of a circular cylinder, to a ($2a$) behavior which is representative of PO scattering from a strip. On the left side of the figure, where $\nu = 2$, the backscattered field of a circular cylinder as a function of radius is seen by the intersection of the curves with the leftmost y-axis. The $\sqrt{a/2}$ behavior is evident. On the right side of the figure, as ν gets large, the field approaches that of the backscattered field from the broad side of a rectangular cylinder. As a function of radius, the intersection of the curves with the rightmost y-axis shows the $2a$ behavior expected from a flat aperture. Because Equation 5.26 is only valid for the backscattered field from the pole, Figure 6.1 does not provide information about the field pattern away from the pole.

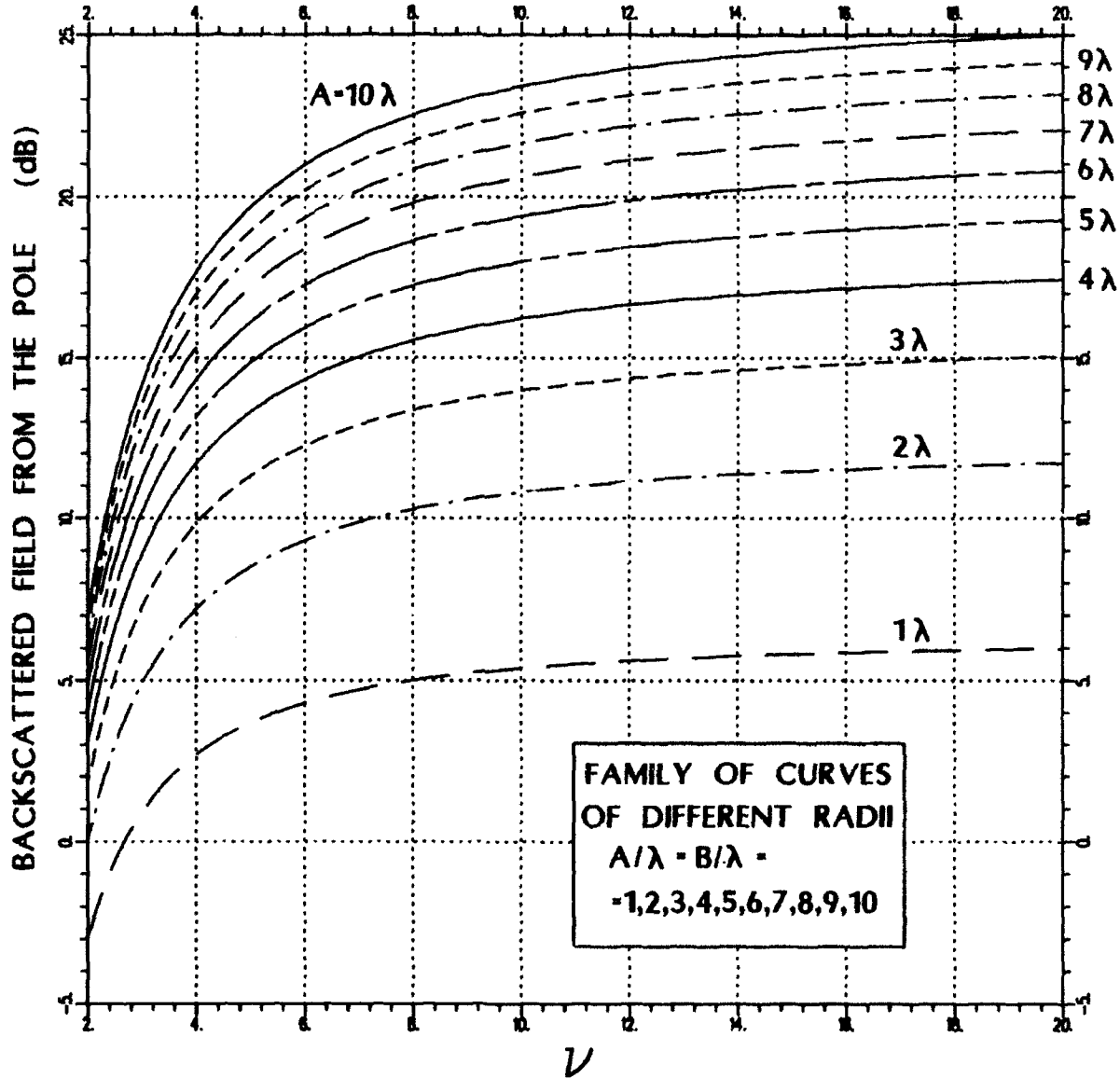

Figure 6.1: Backscattered field from the pole for different radii as a function of ν.

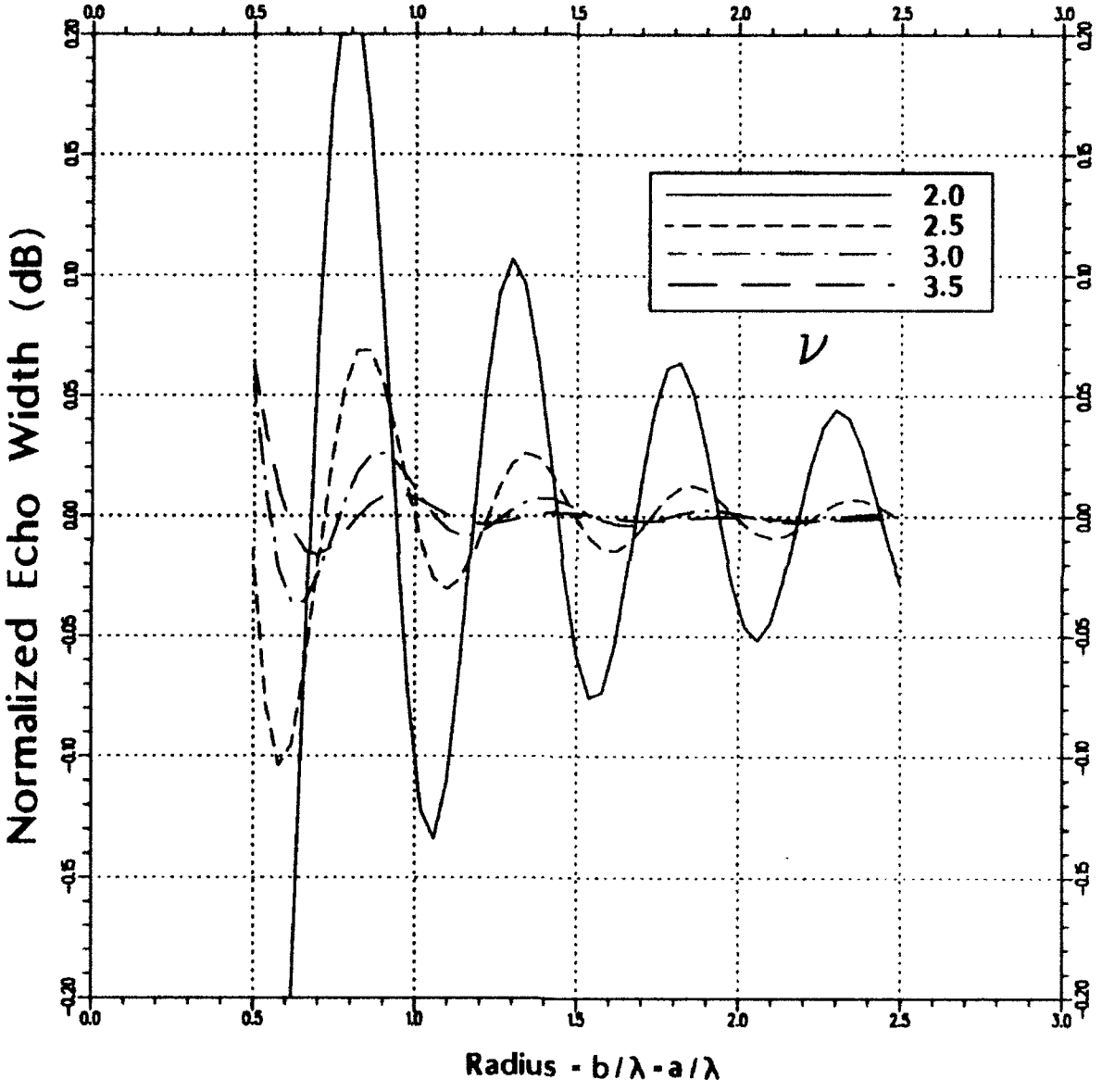

Figure 6.2: Echo width/πa from the pole as a function of radius.

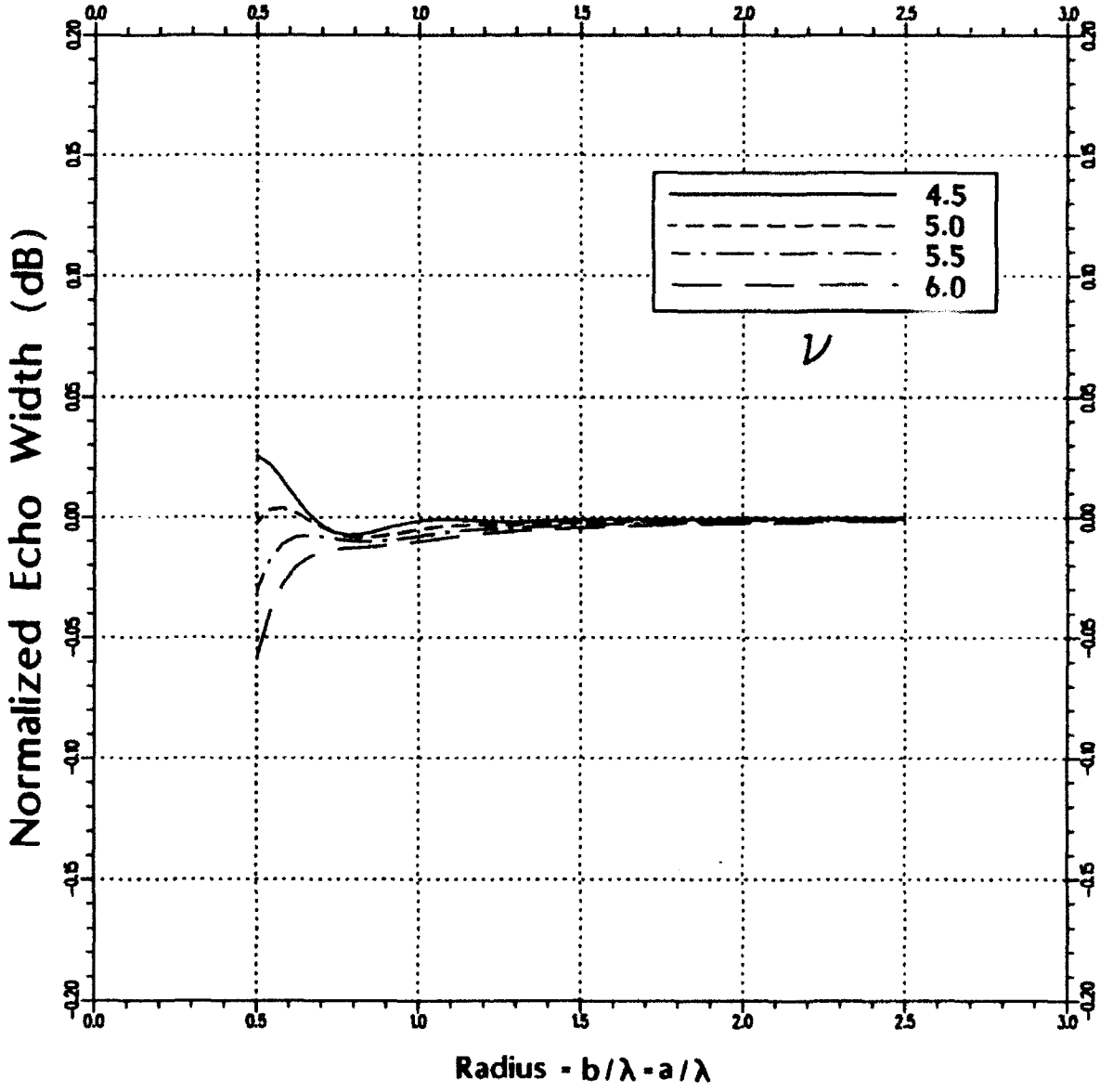

Figure 6.3: Echo width/πa from the pole as a function of radius.

In Figures 6.2 and 6.3, the PO results of Chapter 4 for the TE polarization are displayed on a magnified scale, normalized against the asymptotic results of Equation 5.26 and Figure 6.1. Since the data were generated using numerical integration, the endpoint effects of the false PO termination currents make themselves visible by the observed periodic oscillations. Note that the endpoint effects diminish both as the radius increases and as ν increases. Also note that the scales represent 0.2 dB fluctuations which accentuate this effect.

The decrease of the endpoint effects with increasing radius is a statement of the fact that, with valid assumptions about the PO currents and the surface reflection mechanism, a PO result approaches GO in the limit of infinite frequency. Analytically, PO endpoint contributions usually decrease as $O(1/k)$, where the stationary-phase terms are typically $O(1)$.

The decrease of the endpoint effects with increasing ν is a more subtle effect, but is easily explained. When ν is large, the cylinder is approximately a rectangle but not exactly. The current terminations do not occur at the corners, as in the case of an actual rectangle, but the constant-phase radiation region of the surface does end there. Instead of an abrupt current termination, there is a rapidly fluctuating phase and gradually decreasing current amplitude on the top and bottom sides of the rectangle. This generates a much smaller false return than a current termination immediately adjacent to the constant-phase large-amplitude face of the rectangle.

The validity of Equation 5.26 is indirectly confirmed by the fact that the curves for all ν tend toward zero dB with increasing radius. If Equation 5.26 were inaccurate, then it would not normalize the numerical integration

to unity (0 dB). Also, if all endpoint effects were subtracted out, then all the curves should lie flat on the zero dB line, without oscillation. Again, it must be noted that the amplitude scale in both Figure 6.2 and 6.3 has been *greatly* exaggerated to display the termination current artifacts.

6.2 Reflected Fields from $\nu = 3$ Superelliptic Cylinders

This section presents data for the backscattered fields from superquadric cylinders of $\nu = 3$. Here, the fields are investigated for reflection points both near and far from the pole, and several methods are plotted together for comparison. Unless otherwise noted, the Method of Moments results are for the TM polarization, in order to minimize the effect of creeping waves around the cylinder. Figure 6.5 is the exception, which shows both the TM and TE results using the Method of Moments.

The data are plotted as (echo widths)/πa. This means that the data are normalized to the 2-D echo width of an infinite circular cylinder of radius a. Figure 6.4 shows the backscattered field as a function of the angle from the x-axis for a cylinder of radius $a/\lambda = b/\lambda = 1$.

The GO result is significantly different from the other curves in virtually all regions, and it is the only curve that is unbounded. Note that the UGO and the PO results are almost indistinguishable around the main beam. The UGO and the Method of Moments differ by less than 1/2 dB over the entire angular range. It is worth noting that $a/\lambda = b/\lambda = 1$ is the worst possible case, where the various mechanisms and effects such as creeping

waves and false PO returns are most significant. When the electrical size of the cylinder increases, then UGO and the other methods converge. This includes GO when the reflection point is far from the pole. (Section 5.5 and Equation 5.87 define "near" and "far" from the pole.)

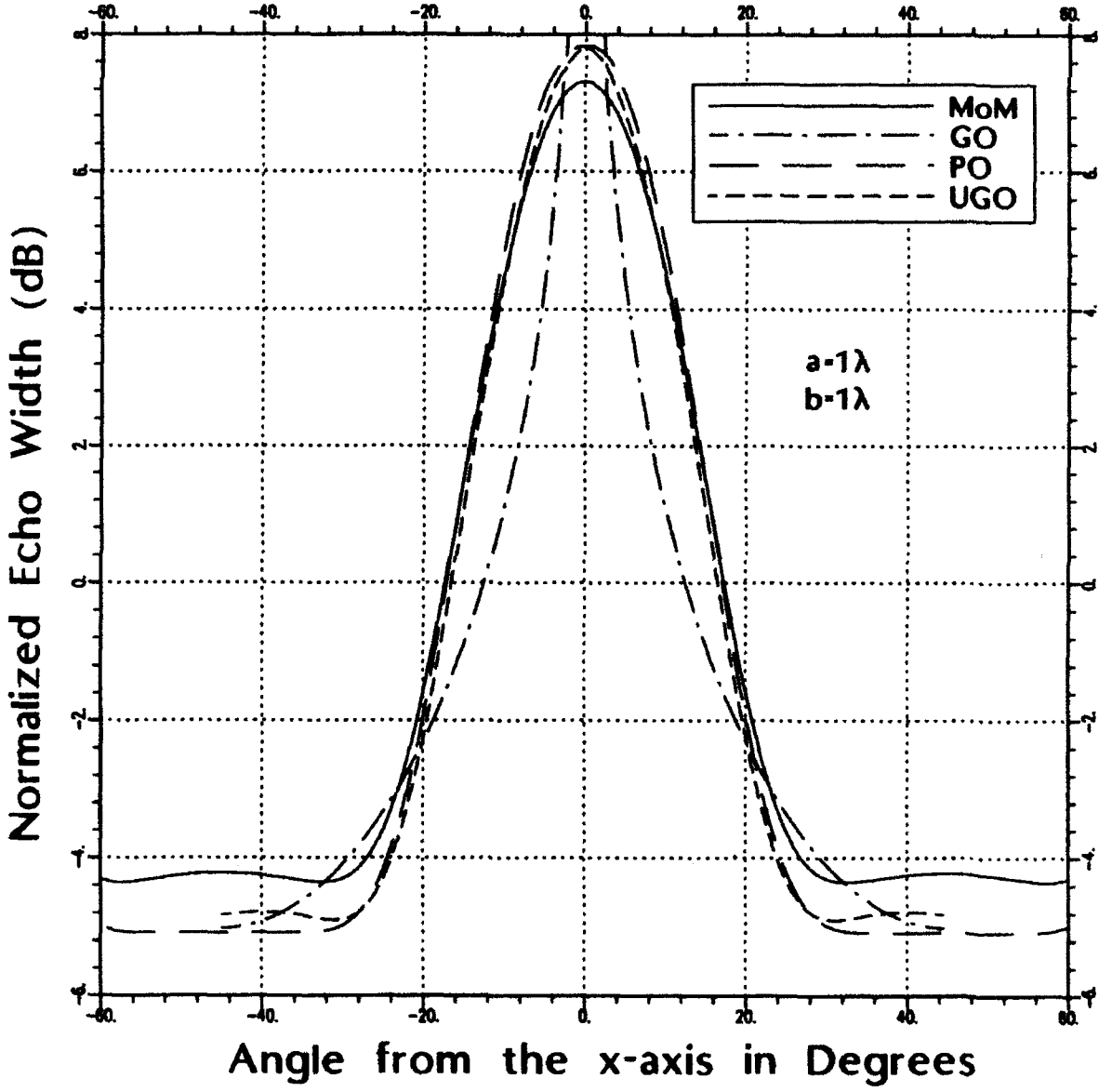

Figure 6.4: Echo width/πa as a function of $\theta = \theta'$, $(a/\lambda = b/\lambda = 1)$.

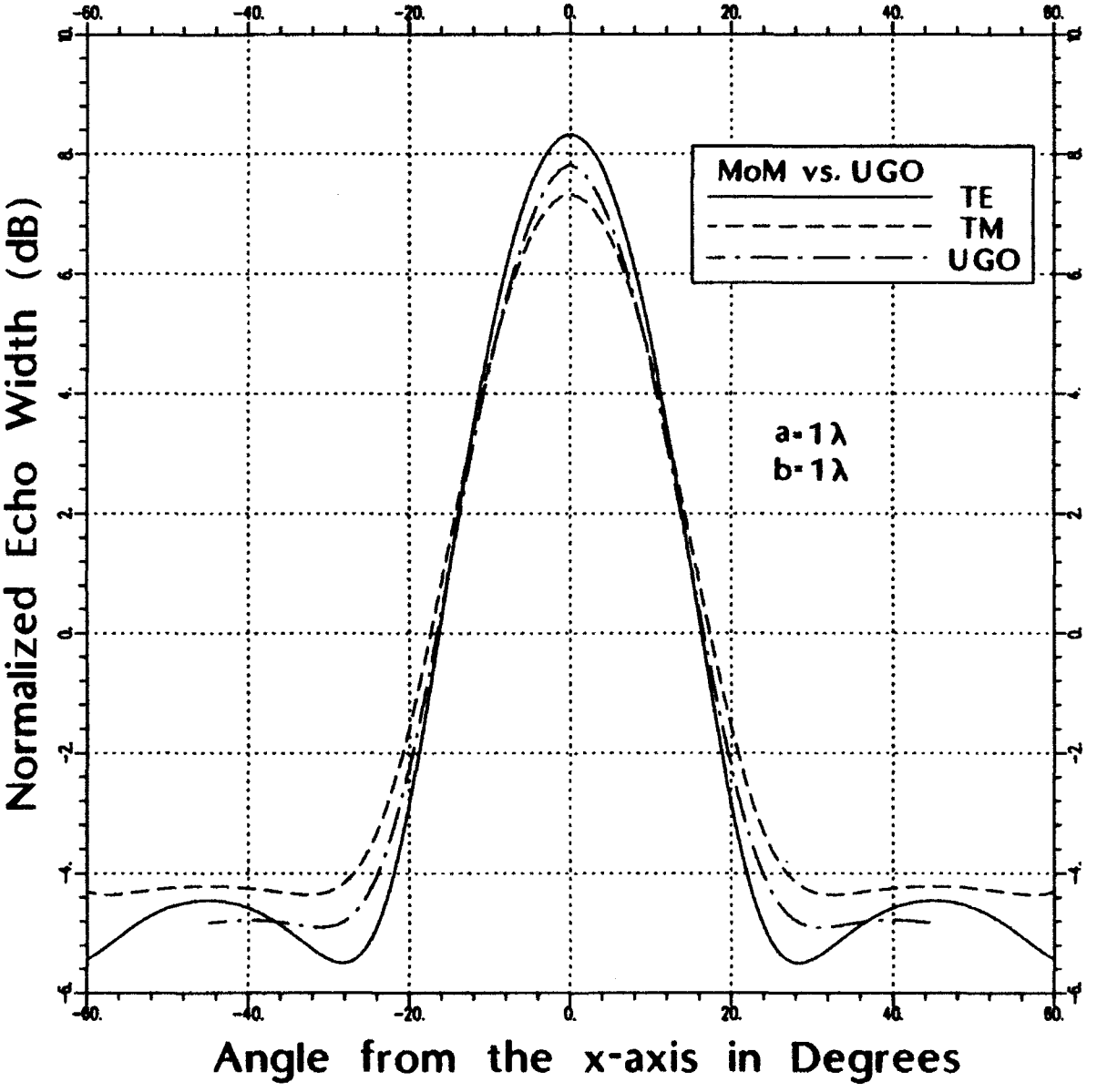

Figure 6.5: Echo width/πa, showing both TM and TE polarizations.

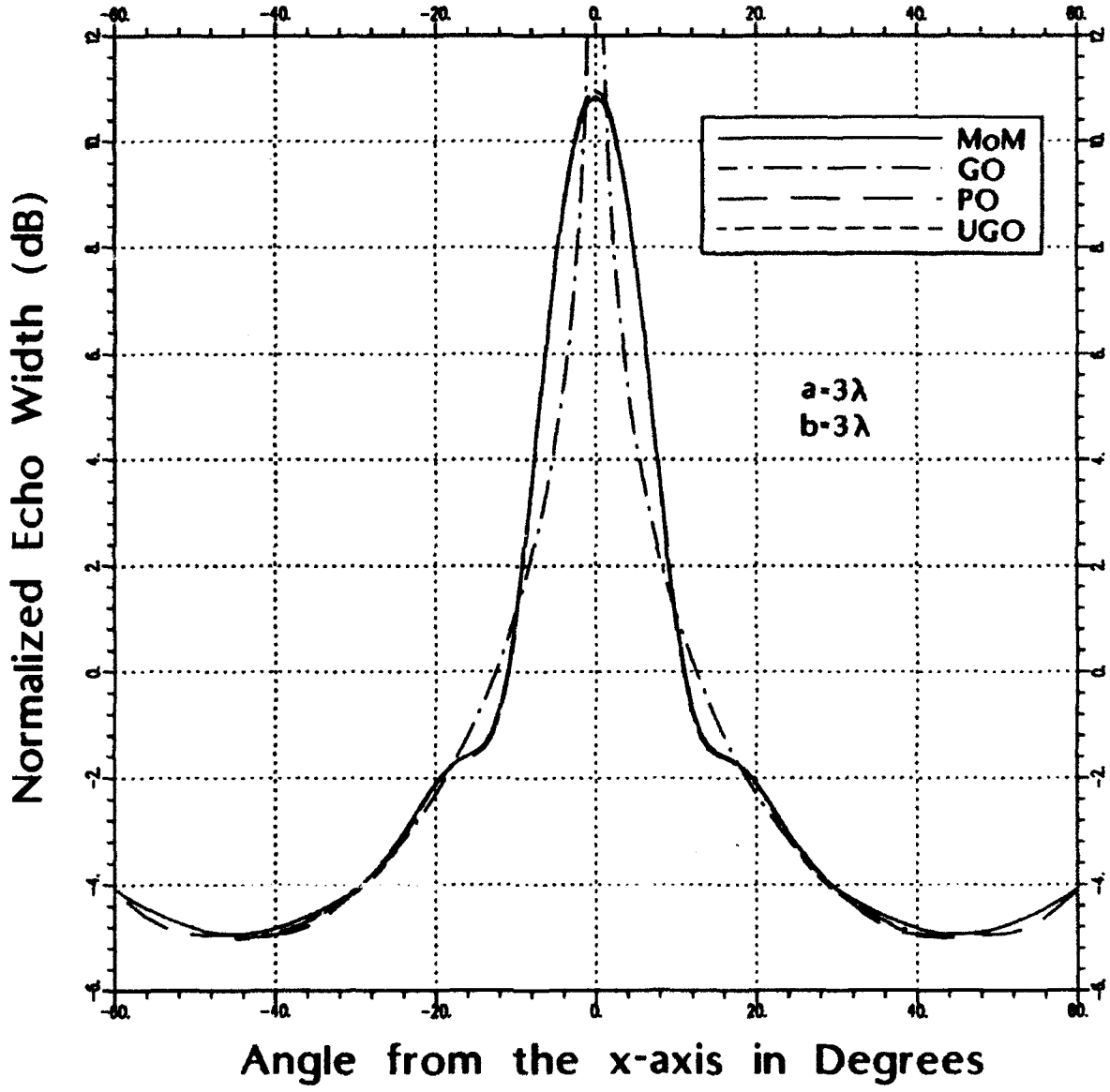

Figure 6.6: Echo width/πa as a function of $\theta = \theta'$, $(a/\lambda = b/\lambda = 3)$.

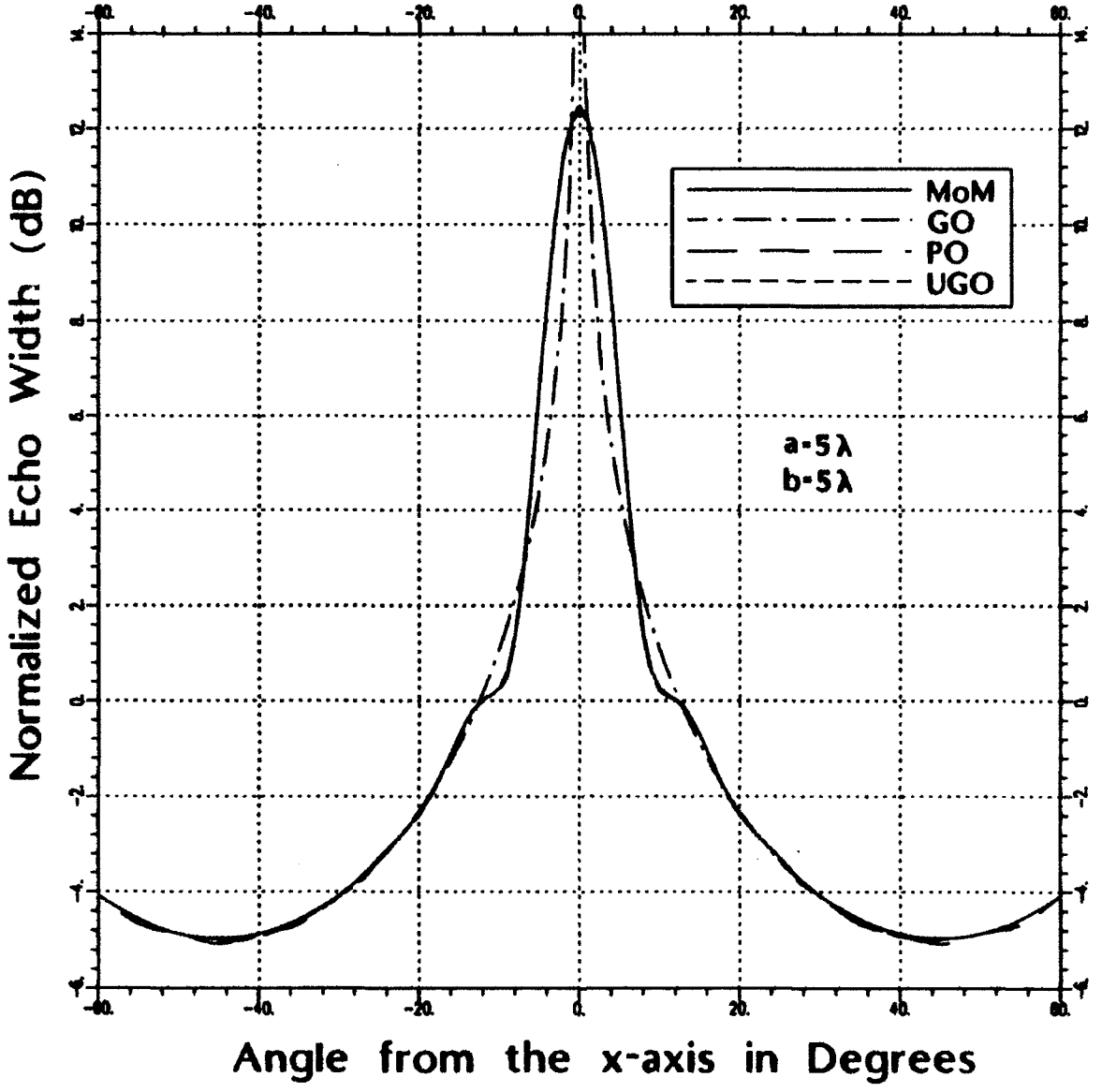

Figure 6.7: Echo width/πa as a function of $\theta = \theta'$, $(a/\lambda = b/\lambda = 5)$.

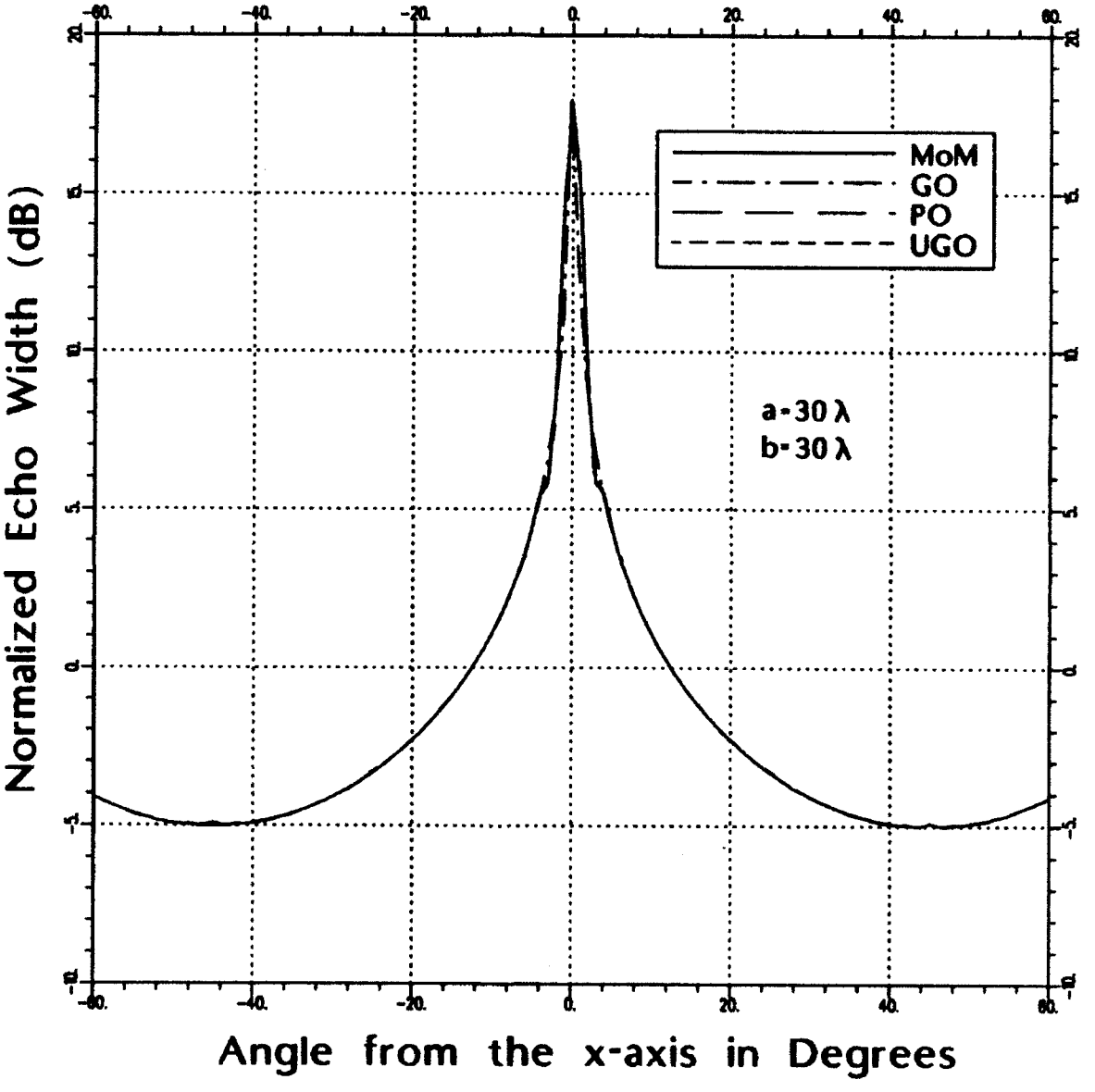

Figure 6.8: Echo width/πa as a function of $\theta = \theta'$, $(a/\lambda = b/\lambda = 30)$.

In Figure 6.5, at the pole, the TM polarization via Method of Moments is 1/2 dB below the UGO, whereas the TE polarization via MoM is 1/2 dB above the UGO figure. Slight discrepancies are also noticeable around the 45 degree mark. The TE case should show stronger creeping wave effects for small radii. This could explain part of the discrepancy. Higher order terms in the asymptotic analysis could also account for these effects. In any case, the comparisons are quite close considering the small amount of deviation, thereby, validating the results.

The differences between PO and UGO in Figures 6.4 and 6.6 - 6.8 can be explained by the termination current artifacts present in the PO solution, which are absent in the UGO. The UGO solution then, is the pure reflection mechanism, inasmuch as the PO can accurately model the primary radiating (stationary-phase) currents on the surface.

As the radius increases, the adverse effects diminish and the UGO result proves to be very accurate indeed. Figure 6.6 shows that for $a/\lambda = b/\lambda = 3$, the UGO and TM-MoM results differ by less that 0.2 dB over the entire angular range. Larger radii cases in Figures 6.7 and 6.8 show even closer agreement between the various methods.

Chapter 7

SUMMARY AND CONCLUSIONS

Superquadric surfaces have points of zero curvature at which GO incorrectly predicts an infinite reflected field. The actual reflected field is finite and is well approximated by the method of Physical Optics. Rather than simply employ PO, however, a correction to the GO solution is constructed via an asymptotic analysis of the PO formulation for the reflected field. The purpose of the asymptotic analysis is to achieve an improvement over PO by avoiding the false returns associated with the truncation of currents at shadow boundaries and by avoiding numerical integration over electrically large bodies. In the spirit of UTD then, the goal is to retain the advantages of GO in terms of calculation efficiency and analytic simplicity while simultaneously enjoying the accuracy and physical insight afforded by the Physical Optics, hence the uniform GO, or UGO solution.

The numerical results of Chapter 6 show excellent agreement between the UGO solution developed here and the Method of Moments. There is also excellent agreement between Physical Optics and the Method of Mo-

ments, validating the inital assumption that PO is a good way to describe the reflection mechanism. In most of the regions where PO and the Method of Moments disagree, the corrected GO solution more closely agrees with the Method of Moments. This reveals that the UGO solution avoids the false current termination effects which afflict the PO result. One exception to this is when the Method of Moments includes a significant higher order scattering mechanism in addition to the reflected field, such as the creeping wave. In this case, the UGO solution does not include this effect.

Finally, the issue of scattering by superellipses in three dimensions is suggested as an interesting area for future research. This would be the next natural step toward making superquadric surfaces into a viable electromagnetic modeling tool.

Bibliography

[1] Abramowitz, M., and Stegun, I. A., editors, *Handbook of Mathematical Functions*, New York: Dover Publications, Inc., p. 446-452, 1972.

[2] Barr, A. H. "Superquadrics and Angle Preserving Transformations," *IEEE Computer Graphics and Applications*, Vol. 1, p.11-23, Jan. 1981.

[3] Bleistein, N. and Handelsman R.A, *Asymptotic Expansions of Integrals*, Dover Publications, Inc., pp. 252-280, 1986.

[4] Burnside, W. D., Dominek A. K., Peters, L., Jr., "A Reflection Ansatz for Surfaces with Electrically Small Radii of Curvature," *Proc. IEEE*, Vol. AP-35, No. 6, p.690-697, June 1987.

[5] Dominek, A., Personal Communication, The Ohio State University ElectroScience Laboratory, Department of Electrical Engineering.

[6] Felsen, L.B. and Macuvitz, N., *Radiation and Scattering of Waves* Prentice-Hall, Inc., pp. 370-388, 1973.

[7] Felsen, L.B. and Macuvitz, N., *Radiation and Scattering of Waves* Prentice-Hall, Inc., pp. 423-428, 1973.

[8] Harrington, R. F., *Time Harmonic Electromagnetic Fields*, McGraw-Hill, Inc., p. 37, 1961.

[9] Harrington, R. F., *Time Harmonic Electromagnetic Fields*, McGraw-Hill, Inc., p. 229, 1961.

[10] Kouyoumjian, R. G , and P. H. Pathak, "A Uniform Geometrical Theory of Diffraction for an Edge in a Perfectly Conducting Surface," *Proc. IEEE*, Vol. 62, pp. 1448-1461, Nov. 1974.

[11] Kouyoumjian, R. G., *EE 819 Class Notes.*

[12] Liang, M. C., Pathak, P. H., "On a Uniform Geometrical Optics Analysis Valid Across Smooth Caustics of Rays Reflected by Smoothly Indented Boundaries", Technical Report 716611-3, The Ohio State University ElectroScience Laboratory, Department of Electrical Engineering, June 1987.

[13] Marhefka, R. J., Personal Communication, The Ohio State University ElectroScience Laboratory, Department of Electrical Engineering.

[14] Marhefka, R. J. and Burnside, W. D., "Numerical Electromagnetic Code - Basic Scattering Code, NEC-BSC (Version 2), Part I: User's Manual," Technical Report 712242-14, The Ohio State University ElectroScience Laboratory, Department of Electrical Engineering; prepared under Contract No. N00123-79-C-1469 for Naval Regional Contracting Office, December 1982.

[15] Marhefka, R. J., "Numerical Electromagnetic Code - Basic Scattering Code, NEC-BSC (Version 2), Part II: Code Manual," Technical Report 712242-15, The Ohio State University ElectroScience Laboratory, Department of Electrical Engineering; prepared under Contract No. N00123-79-C-1469 for Naval Regional Contracting Office, December 1982.

[16] Wang, N. M., "Reaction Formulation for Radiation and Scattering from Plates, Corner Reflectors and Dielectric-coated Cylinders", Technical Report 2909-15, The Ohio State University ElectroScience Laboratory, Department of Electrical Engineering, April 1974.

Appendix A

COMPLETE AND INCOMPLETE AIRY FUNCTIONS

The Airy Functions satisfy a second-order differential equation known as Airy's Differential Equation A.2,A.3,A.23. The integral solutions of these equations are known as Airy integrals and their properties are well known. The structure of the Airy integrals is such that they are characteristic of the arbitrary interaction of two saddle points, and in the case of the incomplete Airy integral they describe the interactions of two saddle points with an endpoint of integration.

This appendix presents the definitions and asymptotic forms of the complete and incomplete Airy functions. While the Complete Airy Functions are not a part of the solutions presented in Chapter 5, they are used in the numerical evaluation of the Incomplete Airy Functions. Asymptotic formulas for the Airy integral are given in [1].

A.1 Complete Airy Functions

A.1.1 Integral Representation

The Complete Airy functions Ai and Bi are defined as

$$\begin{aligned} \mathrm{Ai}(\eta) &= \frac{1}{2\pi j}\int_{L_1} e^{(\eta z - \frac{z^3}{3})}\,dz &&= \frac{1}{2\pi}\int_{L_1} e^{j(\eta s + \frac{s^3}{3})}\,ds \\ \mathrm{Bi}(\eta) &= \frac{1}{2\pi}\int_{L_2+L_3} e^{(\eta z - \frac{z^3}{3})}\,dz &&= \frac{j}{2\pi}\int_{L_2+L_3} e^{j(\eta s + \frac{s^3}{3})}\,ds \end{aligned} \qquad \text{(A.1)}$$

where the contours $L_{1,2,3}$ are shown in Figure A.1.

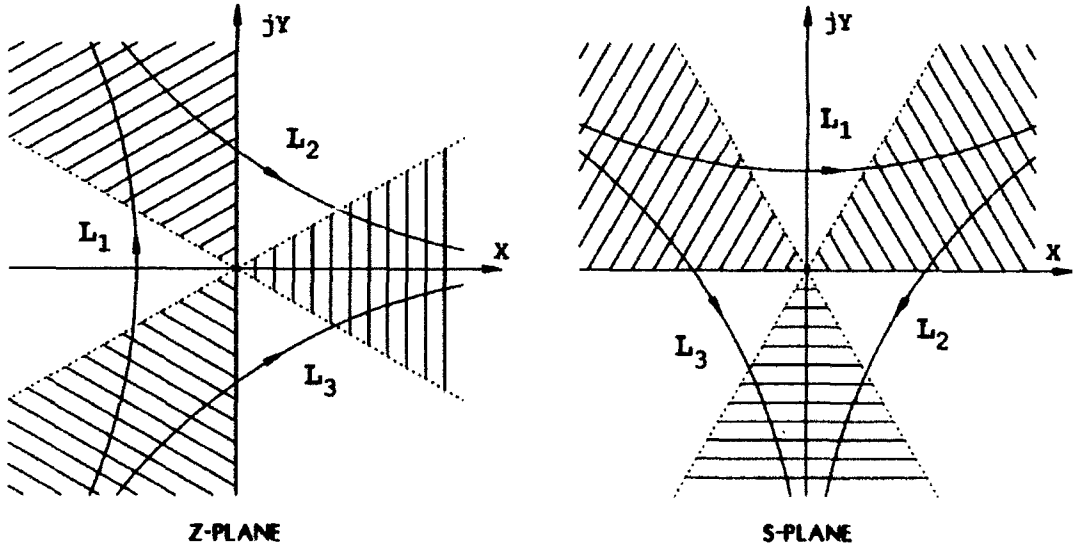

Figure A.1: Contours of integration for the Complete Airy functions

A.1.2 Differential Equations

$$\mathrm{Ai}''(z) - z\mathrm{Ai}(z) = 0. \tag{A.2}$$

$$\mathrm{Bi}''(z) - z\mathrm{Bi}(z) = 0. \tag{A.3}$$

A.1.3 Series Representations

$$\mathrm{Ai}(z) = c_1 f(z) - c_2 g(z) \tag{A.4}$$

$$\mathrm{Bi}(z) = \sqrt{3}\,[c_1 f(z) + c_2 g(z)] \tag{A.5}$$

$$f(z) = \sum_{k=0}^{\infty} 3^k \left(\frac{1}{3}\right)_k \frac{z^{3k}}{(3k)!} \tag{A.6}$$

$$= 1 + \frac{1}{3!}z^3 + \frac{1\cdot 4}{6!}z^6 + \frac{1\cdot 4\cdot 7}{9!}z^9 + \cdots \tag{A.7}$$

$$g(z) = \sum_{k=0}^{\infty} 3^k \left(\frac{2}{3}\right)_k \frac{z^{3k+1}}{(3k+1)!} \tag{A.8}$$

$$= z + \frac{2}{4!}z^3 + \frac{2\cdot 5}{7!}z^7 + \frac{2\cdot 5\cdot 8}{10!}z^{10} + \cdots \tag{A.9}$$

$$\left(\alpha + \frac{1}{3}\right)_0 = 1 \tag{A.10}$$

$$3^k\left(\alpha + \frac{1}{3}\right)_0 = (3\alpha+1)(3\alpha+4)\cdots(3\alpha+3k-1) \tag{A.11}$$

Where α is arbitrary and $k = 1, 2, 3, \cdots$

$$c_1 = \mathrm{Ai}(0) = \mathrm{Bi}(0)/\sqrt{3} = 3^{-2/3}/\Gamma(2/3)$$

$$= 0.355028053887817 \tag{A.12}$$

$$c_2 = -\mathrm{Ai}'(0) = \mathrm{Bi}'(0)/\sqrt{3} = 3^{-1/3}/\Gamma(1/3)$$

$$= 0.258819403792807 \tag{A.13}$$

A.1.4 Large Argument Forms

$$\text{Ai}(z) \sim \text{for } |arg\, z| < \pi, \quad \frac{z^{-1/4}}{2\sqrt{\pi}} e^{-\frac{2}{3}z^{3/2}} \sum_{k=0}^{\infty} (-1)^k \frac{\Gamma(3k+\frac{1}{2})}{54^k k! \Gamma(k+\frac{1}{2})} \left(\frac{2}{3} z^{3/2}\right)^{-k} \tag{A.14}$$

$$\text{Bi}(z) \sim \text{for } |arg\, z| < \tfrac{\pi}{3}, \quad \frac{z^{-1/4}}{\sqrt{\pi}} e^{+\frac{2}{3}z^{3/2}} \sum_{k=0}^{\infty} (-1)^k \frac{\Gamma(3k+\frac{1}{2})}{54^k k! \Gamma(k+\frac{1}{2})} \left(\frac{2}{3} z^{3/2}\right)^{-k} \tag{A.15}$$

A.1.5 Relations between Solutions

$$\text{Bi}(z) - e^{+j\pi/6}\text{Ai}(ze^{j2\pi/3}) + e^{-j\pi/6}\text{Ai}(ze^{-j2\pi/3}) = 0 \tag{A.16}$$

$$\text{Ai}(z) + e^{j2\pi/3}\text{Ai}(ze^{j2\pi/3}) + e^{-j2\pi/3}\text{Ai}(ze^{-j2\pi/3}) = 0 \tag{A.17}$$

$$\text{Bi}(z) + e^{j2\pi/3}\text{Bi}(ze^{j2\pi/3}) + e^{-j2\pi/3}\text{Bi}(ze^{-j2\pi/3}) = 0 \tag{A.18}$$

$$2\,\text{Ai}(ze^{\pm j2\pi/3}) = e^{\pm j2\pi/3}\left[\text{Ai}(z) \pm \text{Bi}(z)\right] \tag{A.19}$$

A.2 Incomplete Airy Functions

The Incomplete Airy functions are defined as

$$G_i(\eta,\beta) = \frac{1}{2\pi}\int_{\beta_i}^{\infty e^{j\psi_i}} e^{j(\eta s+\frac{s^3}{3})}\,ds, \quad i=1,2,3$$
$$= \frac{1}{2\pi j}\int_{j\beta_i}^{\infty j e^{j\psi_i}} e^{(\eta z-\frac{z^3}{3})}\,dz \tag{A.20}$$

$$0 \le \psi_1 \le \tfrac{\pi}{3}, \qquad \tfrac{2\pi}{3} \le \psi_2 \le \pi, \qquad -\tfrac{2\pi}{3} \le \psi_3 \le -\tfrac{\pi}{3} \tag{A.21}$$

where the $\infty e^{j\psi_i}$ and β_i correspond to the endpoints of the S-plane paths L_i shown in Figure A.2. The contour L_1 may be deformed onto the positive

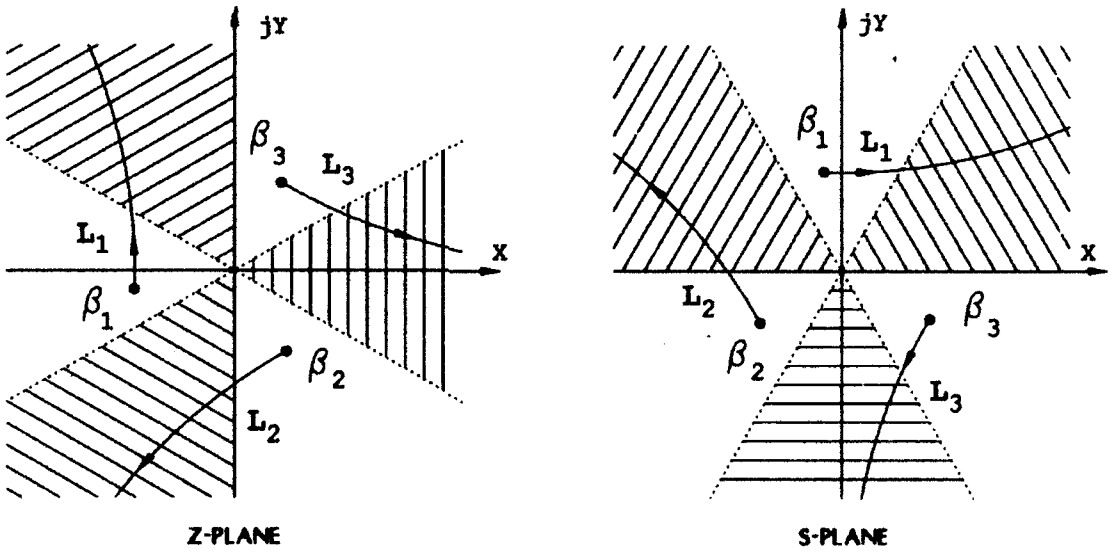

Figure A.2: Contours of integration for the Incomplete Airy functions

real axis in the S-plane to yield the following representation of G_1, denoted

by $\overline{\mathrm{Ai}}$

$$\overline{\mathrm{Ai}}(\eta,\beta) \equiv G_1(\eta,\beta) = \frac{1}{2\pi}\int_{\beta}^{\infty} e^{j(\eta s+\frac{s^3}{3})}\,ds = \frac{1}{2\pi j}\int_{j\beta}^{j\infty} e^{(\eta z-\frac{z^3}{3})}\,dz. \quad \text{(A.22)}$$

A.2.1 Differential Equation

$$\left[\frac{\partial^2}{\partial z^2} - z - j\frac{\partial}{\partial\beta}\right]\overline{\mathrm{Ai}}(z,\beta) = 0 \quad \text{(A.23)}$$

A.2.2 Large Argument Forms

Assume that $\beta \geq 0$ and $x >> 0$.

$$\overline{\mathrm{Ai}}(x,\beta) \sim \frac{j}{2\pi}\frac{e^{j(\frac{1}{3}\beta^3+x\beta)}}{\beta^2+x}; \qquad \beta^2+x >> 0 \quad \text{(A.24)}$$

$$\overline{\mathrm{Ai}}(-x,\beta) \sim \frac{1}{2\pi}e^{-j\frac{2}{3}x^{3/2}} \left[\left(g(0)-\frac{g''(0)}{4j}\right)\int_{\alpha}^{\infty} e^{js^2}\,ds - \frac{g(\alpha)-g(0)}{2j\alpha}e^{j\alpha^2}\right] \quad \text{(A.25)}$$

where

$$g(s) = \frac{dt}{ds} = \frac{2s}{t^2-x}$$

$$g'(s) = \frac{1}{s}\left[g(s) - tg^3(s)\right] \quad \text{(A.26)}$$

$$g''(s) = \frac{1}{s^2}\left[3t^2g^5(s) - 3tg^3(s) - sg^4(s)\right] \quad \text{(A.27)}$$

$$g(0) = \frac{1}{x^4}$$

$$g'(0) = -\frac{1}{3x}$$

$$g''(0) = \frac{5}{12x^{7/4}}$$

$$s_\alpha = \left(\frac{\beta^3}{3} - x\beta + \frac{2}{3}x^{3/2}\right)^{1/2}$$

$$\alpha = \pm s_\alpha \text{ for } \pm(\beta - x^{1/2})$$

A.2.3 Relations between Solutions

$$G_2(\eta,\beta) = G_1(\eta,\beta) - \mathrm{Ai}(\eta) \tag{A.28}$$

$$G_3(\eta,\beta) = G_1(\eta,\beta) - \frac{1}{2}\left[\mathrm{Ai}(\eta) + j\mathrm{Bi}(\eta)\right] \tag{A.29}$$

$$= G_2(\eta,\beta) + \frac{1}{2}\left[\mathrm{Ai}(\eta) - j\mathrm{Bi}(\eta)\right] \tag{A.30}$$

$$\mathrm{Ai}(\eta) = G_1(\eta,\beta) + G_1^*(\eta^*,\beta) \tag{A.31}$$

$$G_1(\eta e^{+j2\pi/3},\beta) = e^{-j2\pi/3} G_2(\eta,\beta e^{+j2\pi/3}) \tag{A.32}$$

$$G_1(\eta e^{-j2\pi/3},\beta) = e^{+j2\pi/3} G_3(\eta,\beta e^{-j2\pi/3}) \tag{A.33}$$

$$G_2(\eta e^{+j2\pi/3},\beta) = e^{-j2\pi/3} G_3(\eta,\beta e^{+j2\pi/3}) \tag{A.34}$$

$$G_2(\eta e^{-j2\pi/3},\beta) = e^{+j2\pi/3} G_1(\eta,\beta e^{-j2\pi/3}) \tag{A.35}$$

$$G_3(\eta e^{+j2\pi/3},\beta) = e^{-j2\pi/3} G_1(\eta,\beta e^{+j2\pi/3}) \tag{A.36}$$

$$G_3(\eta e^{-j2\pi/3},\beta) = e^{+j2\pi/3} G_2(\eta,\beta e^{-j2\pi/3}) \tag{A.37}$$

Appendix B

COMPUTER PROGRAMS

This appendix contains the various computer programs used to calculate the reflected fields from the superelliptic cylinder. Some of the Airy function subroutines were contributed by M. C. Liang.

PROGRAM UNIFORM GO

This program calculates the reflected field from the superellipse using Uniform GO, or UGO.

```
      options /extend_source
      program go
!
!     This program calculates the GO backscattered field from a
!     superellipse.
!
      parameter pi = 3.141592654
      real theta, r_c, Hgo, a, b, knu, area, Refpnt, zs, zc, t, tp

      real x, xxx
      complex transition
```

```
      external r_c, transition

      Refpnt(theta) = atan(sign(abs(
     +          ((b/a)**knu)*tan(theta))**(1/(knu-1)),tan(theta)))

      Hgo ( theta ) = sqrt ( r_c( Refpnt(theta), a, b, knu )/2 )
*
      knu = 3.0

      type*, 'Input a'
      accept*, a
      b=a

      do theta=-45, 45, .995
!
! Calculate [ x=sigma*k^(2/3) ]
!
        t = abs(theta * pi/180)
        tp = t
        zs = ( b * sin((t+tp)/2) ) ** (3./2.)
        zc = ( a * cos((t+tp)/2) ) ** (3./2.)

        xxx = zs**(2./3.) * ( 2*cos((t-tp)/2) /
     +          ( zs + zc )**(1/3.) )**(2/3.)

        xxx = min ( xxx*(2*pi)**(2/3.), 24.0 )  ! bug in airy function

                                                ! for large arguments

        area = Hgo( theta*pi/180 ) ! * cabs ( transition(x) )
        area = area**2 * 2*pi / ( pi * a )
        write(6,*) theta, area
      end do

      end
```

SUBROUTINE RC

This subroutine calculates the radius of curvature at a point on the surface of a superelliptic cylinder.

```
      options /extend_source
      real function R_C( phi, a, b, knu )
      real phi, s, c, knu, a, b
      real sa, ca, sam1, cam1, sam2, cam2

      s       = abs( sin(phi) )
      c       = abs( cos(phi) )
      sa      = s ** knu
      ca      = c ** knu
      sam1    = s ** (knu-1)
      cam1    = c ** (knu-1)
      sam2    = s ** (knu-2)
      cam2    = c ** (knu-2)

      R_C = ( ((a**knu)*sam1)**2 + ((b**knu)*cam1)**2 )**(3./2.) / (
     +          (knu-1) *
     +          (a*b)**(knu-1) * ( (a*s)**knu+(b*c)**knu )**(1+1/knu) *
     +          (s*c) **(knu-2) )

      return
      end
```

FUNCTION TRANSITION

This subroutine calculates the value of the transition function $T(x)$.

```
      options /extend_source
```

```
      complex function Transition ( argument )
      complex  iai, j, z
      external iai
      real     pi, argument
      parameter ( pi = 3.141592654, j=(0.,1.) )
*!
      z = iai( 0.0, +argument )
     +    + iai( 0.0, -argument )

      z = conjg(z) * 2 * sqrt(pi) * (abs(argument)**(1./4.))
     +         * exp( -j*2./3.*(abs(argument)**(3./2.)) + j*pi/4 )


      Transition = z
      return
      end
```

PROGRAM POLE BACKSCATTER

This program calculates the backscattered field from the pole of a superelliptic cylider.

```
      program super ellipse pole
      integer n
      real k, c, a, x, y, pi, gamma, btan2, knu, fact, deriv
      complex i, j/(0.,1.)/

      pi = 3.141592654
      k = 2 * pi

      type*, 'input a'
      accept*, a

      do knu=2.0, 20.0, .1

      deriv = - 2 * gamma( knu )      ! -2(alpha-1)!

      i = gamma(1/knu) * 2/knu *
     +          (-gamma(knu+1)/(deriv*j*k*a))**(1/knu)
     +          * cexp(j*k*2*a)
     +          * csqrt(j*k/(2*pi)) * a

      WRITE (6,*) knu, cabs(i), btan2(aimag(i),real(i))*180/pi, i


      end do

      END


      real    function gamma(x)
      integer i
      real    x, fact
```

```
call gmmma ( x, fact,  i )
gamma = fact
return
end
```

PROGRAM PHYSICAL OPTICS

This program was used to calculate the Physical Optics reflected field from the superelliptic cylinder.

```
OPTIONS /EXTEND_SOURCE
PROGRAM BISTATIC PO
INTEGER PIECES, I, N, MAXPNTS
real    btan2
external btan2
COMPLEX*16 C, J, H, z
real    phase
REAL*8 PHI, LOW, HIGH, RE_H, IM_H, RE_RESULT, IM_RESULT, lambda

REAL*8 FMIN, FMAX, FSTEP, F
REAL*8 PI, A, V, K, L, U, H_NORM, fmin, amax, NORM_H, ONE, CDABS

COMMON A, PHI, J, K, V
EXTERNAL RE_H, IM_H
phase(z) = btan2( dimag(z), real(dreal(z)) )*180/pi

ONE = 1.0000000000000000
J = (0.,1.)
PI = 4 * ATAN (ONE)

TYPE*, 'Input the observation angle (degrees)'
ACCEPT*, PHI

TYPE*, 'Input the cylinder radius (meters)'
ACCEPT*, A

TYPE*, 'Input the frequency range [low,high,step](Ghz)'
ACCEPT*, fmin, fmax, fstep

TYPE*, 'Input the superelliptic parameter (knu)'
ACCEPT*, v
```

```
        phi = phi * pi/180
        fmin  = fmin  * 1e9
        fmax  = fmax  * 1e9
        fstep = fstep * 1e9
!
! Loop through several frequencies.
!
        maxpnts = nint( (fmax-fmin)/fstep )
        WRITE(3,*) maxpnts, real(fmin/1e6), real(fstep/1e6)
        DO N=1, MAXPNTS + 1
!
! Change some parameters for each point.
!
C         A = ( (N-1)*(amax-amin)/MAXPNTS + amin )
C         PHI = ( (N-1)*(pi/2)/MAXPNTS + -pi/2 )
!
          f = ( (N-1)*(fmax-fmin)/MAXPNTS + fmin )
          lambda = 299 792 837.1 / f
          k = 2 * pi /( lambda )
          c = 2 * CDSQRT((j*k)/(8*PI))
!
! Calculate the point.
!
          HIGH = PI/2+ATAN( ABS(TAN(PHI))**(1/(V-1))
     +            *SIGN(-ONE,SIN(PHI)) )
          LOW  = HIGH - PI
          H = (0.,0.)
          PIECES = 2 * NINT( A/lambda )
          DO I=1, PIECES
!
           L = (I-1) * ((HIGH - LOW)/PIECES) + LOW
           U = I     * ((HIGH - LOW)/PIECES) + LOW
!
! Integrate the real and imaginary parts of H due to J.
!
           CALL DQG32( L, U, RE_H, RE_RESULT )
```

```
            CALL DQG32( L, U, IM_H, IM_RESULT )
            H = H + CMPLX(RE_RESULT,IM_RESULT)
!
          END DO
          H = H * C * A
!
! Normalize the result against the GO result.
!
          NORM_H = A * PI
          H_NORM = 2 * PI * CDABS( H )**2 / NORM_H
!
! Output the data to a file and notify the user of progress.
!
          WRITE(3,*) 20*log10(cdabs(H)), phase(h)
          TYPE*, N, ' of ', MAXPNTS, ' f=', f/1e9, ' h=',
     +           20*log10(real(abs(h_norm)))
!
        END DO

        CALL STATISTICS
        END
!
! These functions compute the real and imaginary parts of H.
!
        REAL*8 FUNCTION RE_H ( X )
        REAL*8 X, AMP_NUMER, PHASE_NUMER, PHASE_DENOM, AMP_DENOM
        REAL*8 PHI, A, S, C, V, TMP, IM_H, K
        COMPLEX*16 J
        COMMON A, PHI, J, K, V
        LOGICAL REAL /.FALSE./
!
        REAL = .TRUE.
!
! The real and imaginary parts are very similar.
!
        ENTRY IM_H ( X )
!
```

```
        S = SIN(X)
        C = COS(X)
!
! Calculate the numerators of the amplitude and phase functions.
!
        AMP_NUMER = SIN(PHI)*(SIGN(ABS(S)**(V-1),S)) +
     +              COS(PHI)*(SIGN(ABS(C)**(V-1),C))
        PHASE_NUMER = 2 * ( C * COS(PHI) + S * SIN(PHI) )
!
! Build the denominators of the amplitude and phase functions.
!
        TMP = ( ABS(S)**V + ABS(C)**V )
        PHASE_DENOM = TMP**(1/V)
        AMP_DENOM   = PHASE_DENOM * TMP
!
! Now combine the functions.
!
        IF ( REAL ) THEN
          RE_H = (AMP_NUMER/AMP_DENOM) *
     +         COS( K*A*(PHASE_NUMER/PHASE_DENOM) )
        ELSE
          IM_H = (AMP_NUMER/AMP_DENOM) *
     +         SIN( K*A*(PHASE_NUMER/PHASE_DENOM) )
        END IF
!
! Asume imaginary unless the real entry point was taken.
!
        REAL = .FALSE.
        END
```

SUBROUTINE CDQG32

This subroutine performs a complex double-precision Gaussian quadrature numerical integration on a given function.

```
*!+
*!
*! This is a complex double-precision 32-point gaussian quadrature
*! integration routine.  It integrates the function FUNC on a strait

*! line in the complex plane from ZL to ZU.
*!
*!-
      DOUBLE COMPLEX    FUNCTION CDQG32 ( ZL, ZU, FUNC )
      DOUBLE COMPLEX    FUNC, FCT, Y, ZL, ZU
      DOUBLE PRECISION  A, C1, C2, C3, C4, C5, C6, C7, C8, C9, C10

      DOUBLE PRECISION  C11, C12, C13, C14, C15, C16, C17
      DOUBLE PRECISION  X, B1, B2, B3, B4, B5, B6, B7, B8, B9, B10

      DOUBLE PRECISION  B11, B12, B13, B14, B15, B16, B17
      PARAMETER ( A   = 0.5D0 )
      PARAMETER ( C1  = .49863193092474 D0 )
      PARAMETER ( C2  = .49280575577263 D0 )
      PARAMETER ( C3  = .48238112779375 D0 )
      PARAMETER ( C4  = .46745303796886 D0 )
      PARAMETER ( C5  = .44816057788302 D0 )
      PARAMETER ( C6  = .42468380686628 D0 )
      PARAMETER ( C7  = .39724189798397 D0 )
      PARAMETER ( C8  = .36609105937014 D0 )
      PARAMETER ( C9  = .33152213346510 D0 )
      PARAMETER ( C10 = .29385787862038 D0 )
      PARAMETER ( C11 = .25344995446611 D0 )
      PARAMETER ( C12 = .21067563806531 D0 )
      PARAMETER ( C13 = .16593430114106 D0 )
      PARAMETER ( C14 = .11964368112606 D0 )
      PARAMETER ( C15 = .07223598079139 D0 )
```

```
      PARAMETER ( C16 = .024153832843869 D0 )
      PARAMETER ( B1  = .35093050047350 D-2 )
      PARAMETER ( B2  =  .8137197365452 D-2 )
      PARAMETER ( B3  = .12696032654631 D-1 )
      PARAMETER ( B4  = .17136931456510 D-1 )
      PARAMETER ( B5  = .21417949011113 D-1 )
      PARAMETER ( B6  = .25499029631188 D-1 )
      PARAMETER ( B7  = .29342046739267 D-1 )
      PARAMETER ( B8  = .32911111388180 D-1 )
      PARAMETER ( B9  = .36172897054424 D-1 )
      PARAMETER ( B10 = .39096947893535 D-1 )
      PARAMETER ( B11 = .41655962113473 D-1 )
      PARAMETER ( B12 = .43826046502201 D-1 )
      PARAMETER ( B13 = .45586939347881 D-1 )
      PARAMETER ( B14 = .46922199540402 D-1 )
      PARAMETER ( B15 = .47819360039637 D-1 )
      PARAMETER ( B16 = .48270044257363 D-1 )
*!
      FCT ( X ) = FUNC ( ZL + (ZU-ZL)*X )
*!
      Y = ( 0.0, 0.0 )
      Y = Y + B1  * ( FCT(A+C1)  + FCT(A-C1)  )
      Y = Y + B2  * ( FCT(A+C2)  + FCT(A-C2)  )
      Y = Y + B3  * ( FCT(A+C3)  + FCT(A-C3)  )
      Y = Y + B4  * ( FCT(A+C4)  + FCT(A-C4)  )
      Y = Y + B5  * ( FCT(A+C5)  + FCT(A-C5)  )
      Y = Y + B6  * ( FCT(A+C6)  + FCT(A-C6)  )
      Y = Y + B7  * ( FCT(A+C7)  + FCT(A-C7)  )
      Y = Y + B8  * ( FCT(A+C8)  + FCT(A-C8)  )
      Y = Y + B9  * ( FCT(A+C9)  + FCT(A-C9)  )
      Y = Y + B10 * ( FCT(A+C10) + FCT(A-C10) )
      Y = Y + B11 * ( FCT(A+C11) + FCT(A-C11) )
      Y = Y + B12 * ( FCT(A+C12) + FCT(A-C12) )
      Y = Y + B13 * ( FCT(A+C13) + FCT(A-C13) )
      Y = Y + B14 * ( FCT(A+C14) + FCT(A-C14) )
      Y = Y + B15 * ( FCT(A+C15) + FCT(A-C15) )
      Y = Y + B16 * ( FCT(A+C16) + FCT(A-C16) )
```

```
*!
      CDQG32 = (ZU-ZL) * Y
      RETURN
      END
```

FUNCTION INCOMPLETE AIRY

These functions compute values for the Incomplete Airy functions.

```
      complex function iai ( b, x )
      complex iaip, ibi, ibip, z1, z2, z3, z4
      real    b, x
      call aiinc ( b, x, z1, z2, z3, z4 )
      iai  = z1
      return

      entry   iaip
      call aiinc ( b, x, z1, z2, z3, z4 )
      iaip  = z2
      return

      entry   ibi
      call aiinc ( b, x, z1, z2, z3, z4 )
      ibi  = z3
      return

      entry   ibip
      call aiinc ( b, x, z1, z2, z3, z4 )
      ibip = z4
      return
      end

      SUBROUTINE AIINC(BETA,XS,AII,AIIP,AIH,AIHP)
      COMPLEX AII,AIIP,FCT,FINT,CJ,CJP4
      COMPLEX AIH,AIHP,ATEM(1001),ATMP(1001)
      COMPLEX GI,GIP,HI,HIP,AI,AIP,BI,BIP
      COMPLEX CT1,CT2,CT3,CT4,CT5
      COMMON/ERR/ERR1,ERR2,ERR3,ERR4
C
C     APRIL 17, 1986
C     ***************************************************************
```

```
C       *   THIS SUBROUTINE IS USED TO CALCULATE THE INCOMPLETE AIRY  *
C       *   FUNCTION AND ITS DERIVATIVES, THE FUNCTION IS DEFINED AS  *
C       *   AII(B,S)=INT(B,INF,FS)                                    *
C       *   AIIP(BS)=INT(B,INF,CJ*T*FS)                               *
C       *   FS=EXP(CJ*(T**3/3+S*T))/TPI                               *
C       *   NOTE THAT THE AIRY FUNCTION AI IS DEFINED AS              *
C       *   AI(S)=INT(-INF,INF,FS)                                    *
C       ************************************************************
C
C       IARG=1: SMALL NEGATIVE ARGUMENT OR POSITIVE ARGUMENT FORM;
C               WITH BETA >>1
C          =2: LARGE NEGATIVE ARGUMENT FORM( XS <<0);
C               USING THE FRESNEL INTEGRAL (ASYMPTOTIC FORM)
C           =3: SMALL NEGATIVE ARGUMENT OR POSITIVE ARGUMENT FORM;
C               WITH 0< BETA <<1
C           =4: EVALUATE THE INTEGRAL FORM; AIINC(B,S)=AIINC(0,S)
C               -INT(0,B,FS); WHERE FS=EXP(CJ*(0.33*T*T*T+S*T))/TPI
C
C       ICOM=1: IF BETA < 0 ; IN THIS CASE TAKE THE COMPLIMENTARY
C               PART OF AII(BETA,XS);
C               I.E. AII=AI(XS)-AII_*_(ABS(BETA),XS)
C           =0: IF BETA > 0 .
C
        PI=3.14159265359
        TPI=2.*PI
        CJ=(0.,1.)
        CT1=-CJ*PI/4.
```

```
      CJP4=CEXP(CT1)
      QPI=SQRT(PI)
      BET1=ABS(BETA)
      ICOM=0
      IF(BETA.LT.0.)ICOM=1
      IARG=4
      T1=BET1*BET1+XS
      IF(T1.GE.18.)IARG=1
C     IF(BET1.LE.ERR4)IARG=3
      IF(XS.LE.-7.)IARG=2
      CALL GIHI(XS,GI,GIP,HI,HIP,AI,AIP,BI,BIP)
      AIH=0.5*(AI+CJ*GI)
      AIHP=0.5*(AIP+CJ*GIP)
C
      GO TO (100,200,400,400)IARG
100   CONTINUE
C
C     THIS IS THE LARGE BETA FORM; WITH SMALL NEGATIVE XS OR
C     LARGE POSITIVE XS
C
      CT1=CJ*(BET1*BET1*BET1/3.+XS*BET1)
      CT2=CEXP(CT1)
      BBS1=1./(BET1*BET1+XS)
      BBS2=BBS1*BBS1
      BBS4=BBS2*BBS2
      CT3=CJ*BBS1*(1.-(10.*BET1*BET1-2.*XS)*BBS4)
C           CT4=BBS1*BBS2*2.*BET1*(1.-15.*(3.*BET1*BET1-XS)*BBS4)

      CT4=BBS1*BBS2*2.*BET1
      AII=(CT3+CT4)*CT2/TPI
C
C           CT3=CJ*BBS2*(-1.+BBS4*(52.*BET1*BET1-8.*XS))
C           CT4=BBS4*6.*BET1*(-1.+(110.*BET1*BET1-30*XS)*BBS4)
C
      CT3=-CJ*BBS2
      CT4=-BBS4*6.*BET1
      AIIP=(CT3+CT4)*CT2/TPI+CJ*BET1*AII
```

```
          GO TO 900
200       CONTINUE
C
C         THIS IS THE ASYMPTOTIC FORM FOR LARGE NEGATIVE XS;
C         IN THIS CASE THE FUNCTION IS APPROXIMATED BY FRESNEL
C         INTEGRAL
C
C         THE LARGE ARGUMENT IS DECIDED TO BE USED FOR XS< -7.;
C         IN THIS CASE THE ERROR IS ABOUT 0.3% FOR BETA=0.
C
          ABXS=ABS(XS)
          SAXS=SQRT(ABXS)
          SSAX=SQRT(SAXS)
          DEPS=BET1-SAXS
          CT3=-CJ*2.*ABXS*SAXS/3.
          CT4=CEXP(CT3)
C
C         BRANCH INTO LARGE AND SMALL ARGUMENT FORMS
C
          IF(ABS(DEPS).GT.0.03)GO TO 250
C
C         SMALL ARGUMENT FORMS
C
          T1=1.+DEPS/(6.*SAXS)-DEPS*DEPS/(72.*ABXS)
          DEBTA=T1*DEPS*SSAX
          DEBTA2=DEBTA*DEBTA
          CT1=CJ*DEBTA2
          CT2=CEXP(CT1)
          CT1=QPI*(0.7070106781,0.7070106781)
          FINT=0.5*CT1-DEBTA-0.33333334*DEBTA*DEBTA2*CJ
          T1=1.-0.625*DEPS/SAXS+0.3402777778*DEPS*DEPS/ABXS
          CT5=-0.5*CT2*T1*CJ/(ABXS*3.)
          AII=CT4*((1.+CJ*0.10416666667/(SAXS*ABXS))*FINT/SSAX+CT5)/TPI

          T2=1.-0.4375*DEPS/SAXS+0.409722222*DEPS*DEPS/ABXS
          CT5=T2*CT2/(3.*SAXS)
          AIIP=CT4*((CJ+0.1458333333/(SAXS*ABXS))*SSAX*FINT-CT5)/TPI
```

```
          GO TO 900
C
C         LARGE ARGUMENT FORMS
C
250       GEO=1./SSAX
          T1=BET1*BET1*BET1/3.+XS*BET1+2.*SAXS*ABXS/3.
          DEBTA=SQRT(T1)
          IF(BET1.LT.SAXS)DEBTA=-DEBTA
C                GEBTA=GEO
C                T1=BET1*BET1+XS
C                IF(ABS(T1).GE.0001)GEBTA=2.*DEBTA/T1
          GEBTA=2.*DEBTA/(BET1*BET1+XS)
          DEBTA2=DEBTA*DEBTA
          CALL FCTX(1,FCT,DEBTA2)
          CT1=CJ*DEBTA2
          CT2=CEXP(CT1)
          CT1=QPI*(0.7070106781,0.7070106781)
C
          FINT=0.5*CONJG(FCT)*CJ*CT2/DEBTA
          IF(DEPS.LT.0.)FINT=CT1+FINT
C
          CT5=0.5*CJ*(GEBTA-GEO)/DEBTA*CT2
          AII=CT4*((GEO+CJ*0.10416666667*SSAX/(ABXS*ABXS))*FINT+CT5)/TPI

C
          CT5=(BET1/(BET1*BET1+XS)-0.5*SSAX/DEBTA)*CT2
          AIIP=CT4*((CJ*SSAX+0.1458333333/(SSAX*ABXS))*FINT-CT5)/TPI

          GO TO 900
C
C300      CONTINUE
C         BET2=BETA*BETA
C         BET4=BET2*BET2
C         BET8=BET4*BET4
C         XS2=XS*XS
C         XS4=XS2*XS2
```

```
C       T1=BET1-BET1*BET2*(BET4/126.+XS*BET2/15.+XS2/6.)
C       T2=BET2*(BET2/12.+0.5*XS)-(BET4/12.)*(BET4*BET2/135+
C     $ XS*BET4/12.+XS2*BET2/3.+XS*XS2/2.)
C       T3=(BET1*BET4/6.)*(BET8/4212.+XS*BET2*BET4/297.
C     $ +XS2*BET4/54.+XS*XS2*BET2/21.+XS4/20.)+T1
C       AII=AIH-CMPLX(T3,T2)/TPI
C       T4=-(BET1*BET2/3.)*(BET2/5.+XS)+(BET1*BET4/6.)
C     $ *(XS*XS2/5.+XS2*BET2/7.+XS*BET4/27.+BET2*BET4/297.)
C       T5=0.5*BET2*(1.-BET2*BET4/72.-XS*BET4/9.-XS2*BET2*0.25)
C       AIIP=AIHP-CMPLX(T4,T5)/TPI
C       GO TO 900
400     CONTINUE
        N3=25
        IF((BET1.GE.3.).AND.(XS.GE.0.))N3=50
        NNT=BET1*N3+1
        N1=NNT/2
        N2=NNT-N1*2
        IF(N2.EQ.0)NNT=NNT+1
        IF(NNT.LE.3)NNT=3
        DELT=BET1/(NNT-1)
C
        DO 410 I=1,NNT
        T1=DELT*(I-1)
        CT1=CJ*(T1*T1*T1/3.+XS*T1)
        CT2=CEXP(CT1)
        CT3=CJ*T1*CT2
        ATEM(I)=CT2
        ATMP(I)=CT3
410     CONTINUE
C
        N1=(NNT-1)/2
        CT4=(0.,0.)
        CT5=(0.,0.)
        DO 440 J=1,N1
        J1=2*J
        J1M=J1-1
        J1P=J1+1
```

```
          CT4=CT4+(ATEM(J1M)+4.*ATEM(J1)+ATEM(J1P))*DELT/3.
          CT5=CT5+(ATMP(J1M)+4.*ATMP(J1)+ATMP(J1P))*DELT/3.
440       CONTINUE
C
          AII=AIH-CT4/TPI
          AIIP=AIHP-CT5/TPI
900       IF(ICOM.EQ.C)RETURN
C
C         ICOM=0 MEANS THAT BETA > 0;ICOM=1 MEANS THAT BETA < 0.
C
          AII=AI-CONJG(AII)
          AIIP=AIP-CONJG(AIIP)
          RETURN
          END
          SUBROUTINE GIHI(XS,GI,GIP,HI,HIP,AI1,AI1P,BI1,BI1P)
C
C         XS: REAL ARGUMENT
C         GI,GIP,HI,HIP: COMPLEX VARIABLE
C         THIS SUBROUTINE IS USED TO CALCULATE THE GI,HI FUNCTION
C
          COMPLEX AI1,AI1P,BI1,BI1P
          COMPLEX ZS,GI,GIP,HI,HIP,AT1,AT2
          DIMENSION AGT(1001),AGP(1001)
          COMMON ERR1
          PI=3.14159265359
          PI4=PI/4.
          SQPI=SQRT(PI)
          IARG=2.
          IF(XS.GE.4.7)IARG=3
          IF(XS.LE.-9.)IARG=1
C
C         IARG=1: NEGATIVE LARGE ARGUMENT; THE SOLUTION IS OSCILLATING

C         IARG=2: SMALL ARGUMENT; FOR BOTH POSITIVE AND NEGATIVE ARGUMENT

C         IARG=3: POSITIVE LARGE ARGUMENT; THE SOLUTION DAMPING FAST
C
```

```
      T1=ABS(XS)
      T1=SQRT(T1)
      XS14=SQRT(T1)
      XS32=T1*T1*T1
      ZS=CMPLX(XS,0.)
      CALL AIBI(ZS,AI1,AI1P,BI1,BI1P)
      GO TO (100,200,300)IARG
100   CONTINUE
      XS3=XS*XS*XS
      T2=-1./(PI*XS)*(1.+2./XS3+40./(XS3*XS3))
      T3=1./(PI*XS*XS)*(1.+8./XS3+280./(XS3*XS3))
      HI=CMPLX(T2,0.)
      HIP=CMPLX(T3,0.)
      GI=BI1-HI
      GIP=BI1P-HIP
      RETURN
200   CONTINUE
      IF(ABS(XS).NE.0.)GO TO 250
      GI=CMPLX(0.204975542478,0.)
      GIP=CMPLX(0.149429452449,0.)
      HI=2.*GI
      HIP=2.*GIP
      RETURN
250   CONTINUE
C
C     THE INTEGRAL IS CALCULATED USING THE DEFINITE INTEGRAL 0 TO AUG

C     AND THEN ADD UP THE REMAINDER FROM THE REST OF THE INTEGRAL

C     USING ASYMPTOTIC EVALUATION
C
      AUG=4.
      IF(XS.GE.3.)AUG=6.
      IF(XS.LE.-3.)AUG=2.
      AUG2=AUG*AUG
      DELT=0.01
      NNT=AUG/DELT+1
```

```
      DO 280 I=1,NNT
      XT=(I-1)*DELT
      ARG=-XT*XT*XT/3.+XS*XT
      T1=EXP(ARG)
      AGT(I)=EXP(ARG)
      AGP(I)=XT*EXP(ARG)
280   CONTINUE
      N1=(NNT-1)/2
      T2=0.
      T3=0.
      DO 290 J=1,N1
      J1=2*J
      J1M=J1-1
      J1P=J1+1
      T2=T2+(AGT(J1M)+4.*AGT(J1)+AGT(J1P))*DELT/(3.*PI)
      T3=T3+(AGP(J1M)+4.*AGP(J1)+AGP(J1P))*DELT/(3.*PI)
290   CONTINUE
      T4=XS*AUG-AUG*AUG2/3.
      T6=EXP(T4)
      XSTT=1./(XS-AUG2)
      XST2=XSTT*XSTT
      XST4=XST2*XST2
      T7=T6*XSTT*(-1.+2.*AUG*XST2-(2.*XS+10.*AUG2)*XST4)/PI
      T2=T2+T7
      T8=T6*XST2*(1.-6.*AUG*XST2+(8.*XS+52.*AUG2)*XST4)/PI
      T3=T3+4.*T7+T8
      HI=CMPLX(T2,0.)
      HIP=CMPLX(T3,0.)
      GI=BI1-HI
      GIP=BI1P-HIP
      RETURN
300   CONTINUE
      XS3=XS*XS*XS
      T2=1./(PI*XS)*(1.+2./XS3+40./(XS3*XS3))
      T3=-1./(PI*XS*XS)*(1.+8./XS3+280./(XS3*XS3))
      GI=CMPLX(T2,0.)
      GIP=CMPLX(T3,0.)
```

```
          ARG=2.*XS32/3.
          T4=EXP(ARG)
          T5=T4/(SQPI*XS14)
          T6=T4*XS14/SQPI
          HI=CMPLX(T5,0.)
          HIP=CMPLX(T6,0.)
          RETURN
          END

CCC-------------------------------------------------------
          SUBROUTINE FCTX(ID,FCT,X)
          COMPLEX FXX(8),FX(8),CJ,FCT
          DIMENSION XX(8)
          DATA PI,TPI,SML/3.14159265,6.28318531,0.001/
          DATA XX/.3,.5,.7,1.,1.5,2.3,4.,5.5/
          DATA CJ/(0.,1.)/
          DATA FX/(0.5729,0.2677),(0.6768,0.2682),(0.7439,0.2549),
       1(0.8095,0.2322),(0.873,0.1982),(0.9240,0.1577),(0.9658,0.1073),

       2(0.9797,0.0828)/
          DATA FXX/(0.,0.),(0.5195,0.0025),(0.3355,-0.0665),
       1(0.2187,-0.0757),(0.127,-0.068),(0.0638,-0.0506),
       2(0.0246,-0.0296),(0.0093,-0.0163)/
          IF(X.GT.5.5)GO TO 1
          IF(X.GT.0.3)GO TO 10
C
C         ID=1 DIFFRACTION COEFFICIENT FX
C         ID=2 SLOPE DIFFRACTION COEFFICIENT FXS
C
C!!!      SMALL ARGUMENT FORM
          FCT=((1.253,1.253)*SQRT(X)-(0.,2.)*X-0.6667*X*X)*CEXP(CJ*X)

          IF(ID.EQ.2) FCT=2.*CJ*X*(1.-FCT)
          RETURN
C!!!      LINEAR INTERPOLATION REGION
10        DO 11 N=2,7
11        IF(X.LT.XX(N))GO TO 12
```

```
12      FCT=FXX(N)*(X-XX(N))+FX(N)
         IF(ID.EQ.2) FCT=2.*CJ*X*(1.-FCT)
         RETURN
C!!!    LARGE ARGUMENT FORM
1        IF(ID.EQ.1) FCT=1.+CMPLX(-0.75/X,0.5)/X
         IF(ID.EQ.2) FCT=1.+CMPLX(-3.75/X,1.5)/X
         RETURN
         END
```

FUNCTION COMPLETE AIRY

These functions compute values for the Complete Airy functions.

```
      complex function ai ( z )
      complex z, aip, bi, bip, z1, z2, z3, z4
      call aibi ( z, z1, z2, z3, z4 )
      ai  = z1
      return

      entry   aip
      call aibi ( z, z1, z2, z3, z4 )
      aip  = z2
      return

      entry   bi
      call aibi ( z, z1, z2, z3, z4 )
      bi  = z3
      return

      entry   bip
      call aibi ( z, z1, z2, z3, z4 )
      bip = z4
      return
      end

      SUBROUTINE AIBI(Z,AI,AIP,BI,BIP)
      COMPLEX Z,AI,AIP,BI,BIP
      IF(CABS(Z).GT.6.)GO TO 12
      CALL AIBI1(Z,AI,AIP,BI,BIP)
      RETURN
12    CALL AIBI2(Z,AI,AIP,BI,BIP)
      RETURN
      END
      SUBROUTINE AIBI1(Z,AI,AIP,BI,BIP)
C   THIS PROGRAM CALCULATES THE AIRY FUNCTIONS AI(Z),BI(Z),
```

```
C   AND THEIR DERIVATIVES AIP(Z),BIP(Z).
C   REF. ABRAMOWITZ AND STEGUN, HANDBOOK OF MATHEMATICAL FUNCTIONS.

C   FOR CABS(Z) .LE. 6.0 ,A TAYLOR SERIES IS USED.
C   ARG(Z) MAY TAKE ANY VALUE. SEE (10.4.2) TO (10.4.5) .
      COMPLEX Z,AI,AIP,BI,BIP
      COMPLEX*16 F,G,FP,GP
      DOUBLE PRECISION CC1,CC2
      DATA S3,CC1,CC2/1.732050808,.355028053887817,.258819403792807 /

      CALL FZGZ(Z,F,G,FP,GP)
      AI=CC1*F-CC2*G
      AIP=CC1*FP-CC2*GP
      BI=S3*(CC1*F+CC2*G)
      BIP=S3*(CC1*FP+CC2*GP)
      RETURN
      END
      SUBROUTINE FZGZ(Z,F,G,FP,GP)
C   THE AUXILIARY FUNCTIONS F(Z),G(Z),FP(Z),GP(Z) ARE COMPUTED AS IN

C   "TABLES OF THE MODIFIED HANKEL FUNCTIONS OF ORDER ONE-THIRD AND

C   OF THEIR DERIVATIVES",COMPUTATION LAB, HARVARD UNIV. PRESS,1945.

      COMPLEX*16 F,G,FP,GP,Z3,Z3M,ZD
      COMPLEX Z
      REAL*8 AM,BM,CM,DM,A0,B0,C0,D0
      REAL ZMBD(5)
      INTEGER MAX(5)
      DATA ZMBD /6.1, 5.6, 4.8, 4.1, 3.2 /
      DATA MAX /22, 19, 16, 14, 11 /
      ZD=0.D0
      ZD=Z
      A0=1.D0
      B0=1.D0
      C0=0.5D0
      D0=1.D0
```

```
      Z3=(ZD**3)/200
      Z3M=Z3
      ZMAG=CABS(Z)
      DO 3 M=1,5
3     IF(ZMAG .LE. ZMBD(M))MADMAX=MAX(M)
      F=A0
      G=B0
      FP=C0
      GP=D0
      DO 10 M=1,MADMAX
      TM=FLOAT(3*M)
      AM=200.D0*A0/TM/(TM-1)
      BM=200.D0*B0/TM/(TM+1)
      CM=200.D0*C0/TM/(TM+2)
      DM=200.D0*D0/TM/(TM-2)
      F=F+AM*Z3M
      G=G+BM*Z3M
      FP=FP+CM*Z3M
      GP=GP+DM*Z3M
      Z3M=Z3M*Z3
      A0=AM
      B0=BM
      C0=CM
      D0=DM
10    CONTINUE
      G=ZD*G
      FP=(ZD**2)*FP
      RETURN
      END
      SUBROUTINE AIBI2(XX,AI,AIP,BI,BIP)
C     THIS PROGRAM CALCULATES THE AIRY FUNCTIONS AI(XX),BI(XX),
C     AND THEIR DERIVATIVES AIP(XX),BIP(XX).
C     REF. ABRAMOWITZ AND STEGUN, HANDBOOK OF MATHEMATICAL FUNCTIONS.

      COMPLEX Z,AI,AIP,BI,BIP,XX
      COMPLEX Z25,ZTB,ZT,ZT2,ZT3,ZT4,ZT5
      COMPLEX CT1,A2L2,EIPI3,EIPI6,C,S
```

```
      DATA RTPI,TWORPI,RTOP,POF
     %  /1.772453851,3.544907702,.797884561,.785398164 /
      DATA A2L2,EIPI6,EIPI3
     %  /(0.,.346573590),(.866025404,.5),(.5,.866025404) /
      DATA C1/.069444444/,C2/.037133487/,C3/.037993059/,
     %  C4/.057649190/,C5/.116099064/
      DATA D1/-.097222222/,D2/-.043885030/,D3/-.042462830/,
     %  D4/-.062662163/,D5/-.124105896/
      ZTB=(2./3.)*XX**1.5
      ARG=ATAN2(AIMAG(XX),REAL(XX))
      IF(ABS(ARG).GE.2.1) GO TO 100
C EQN. (10.4.59),(10.4.61)
      Z25=XX**.25
      ZT=ZTB
      ZT2=ZT*ZT
      ZT3=ZT2*ZT
      ZT4=ZT2*ZT2
      ZT5=ZT3*ZT2
      CT1=CEXP(-ZT)/TWORPI
      AI=CT1/Z25*(1-C1/ZT+C2/ZT2-C3/ZT3+C4/ZT4-C5/ZT5)
      AIP=-CT1*Z25*(1-D1/ZT+D2/ZT2-D3/ZT3+D4/ZT4-D5/ZT5)
      IF(ARG.LT.0.)GO TO 20
      ZT=(0.,-1.)*ZTB
C EQN. (10.4.65),(10.4.68) WITH UPPER SIGNS.
      Z=XX/EIPI3
      CT1=ZT+POF-A2L2
      BI=EIPI6
      BIP=1./EIPI6
      GO TO 30
20    ZT=(0.,1.)*ZTB
C EQN. (10.4.65),(10.4.68) WITH LOWER SIGNS.
      Z=XX*EIPI3
      CT1=ZT+POF+A2L2
      BI=1./EIPI6
      BIP=EIPI6
30    S=CSIN(CT1)
      C=CCOS(CT1)
```

```
      Z25=Z**.25
      ZT2=ZT*ZT
      ZT3=ZT2*ZT
      ZT4=ZT2*ZT2
      ZT5=ZT3*ZT2
      BI=BI*RTOP/Z25*(S*(1-C2/ZT2+C4/ZT4)-C*(C1/ZT-C3/ZT3+C5/ZT5))

      BIP=BIP*RTOP*Z25*(C*(1-D2/ZT2+D4/ZT4)+S*(D1/ZT-D3/ZT3+D5/ZT5))

      RETURN
100   ZT=(0.,1.)*ZTB
C EQN. (10.4.60),(10.4.62),(10.4.64),(10.4.67)
      IF(ARG.LT.0.)ZT=-ZT
      Z=-XX
      Z25=Z**.25
      ZT2=ZT*ZT
      ZT3=ZT2*ZT
      ZT4=ZT2*ZT2
      ZT5=ZT3*ZT2
      CT1=ZT+POF
      S=CSIN(CT1)
      C=CCOS(CT1)
      AI=1./RTPI/Z25*(S*(1-C2/ZT2+C4/ZT4)-C*(C1/ZT-C3/ZT3+C5/ZT5))

      AIP=-Z25/RTPI*(C*(1-D2/ZT2+D4/ZT4)+S*(D1/ZT-D3/ZT3+D5/ZT5))

      BI=1./RTPI/Z25*(C*(1-C2/ZT2+C4/ZT4)+S*(C1/ZT-C3/ZT3+C5/ZT5))

      BIP=Z25/RTPI*(S*(1-D2/ZT2+D4/ZT4)-C*(D1/ZT-D3/ZT3+D5/ZT5))

      RETURN
      END
```